QATAR UNIVERSITY

College of Engineering

Density Functional Theory Study of Dry Reforming of Methane

By

Abdraman Mahamat Moussa

A Thesis submitted to

the Faculty of the College of

Engineering

in Partial Fulfillments

of the requirements

For the Degree of

Master of Science in Environmental Engineering

January 2018

COMMITTEE PAGE

The members of the Committee approve the thesis of Abdraman Mahamat Moussa defended on 04/12/2017.

Dr. Mohammed Ali H Saleh

Thesis/Dissertation Supervisor

Dr. Majeda Khraisheh

Thesis/Dissertation Co-Supervisor

Dr. Johan JACQUEMIN

Committee Member

Dr. Muftah El-Naas

Committee Member

Approved:

_____

Khalifa Al-Khalifa, Dean, College of Engineering

Abstract

Moussa,Abdraman,M., Masters: January,2018, Master of Science in Environmental Engineering.

Title: Density Functional Theory Study of Dry Reforming of Methane

Supervisors of thesis: Dr. Mohammed H. Saleh, and Prof. Majeda Khraisheh.

In the recent years, the global warming effects are being catastrophic and they start hitting new areas. These effects have a direct relation with the amount of greenhouse gases emitted into the atmosphere. CO_2 and other greenhouse could be utilized as energy sources by capturing and utilizing them. Dry reforming of methane is one of them and it has economic feasibility that can be commercialized.

In this study, density functional theory calculations were performed to study the promising dry reforming process on Ni111 surface by using SIESTA simulation package. SIESTA is considered to be fast reliable way to perform DFT calculations. Moreover, counterpoise correction was used in order to improve the accuracy. The calculations were performed for different potential active sites and orientations.

The dissociation of CH_4 and CO_2 and their possible pathways were investigated in order to understand the kinetic of the process. The first CH_4 dissociation was found to be the hard step to begin with. Horizontal CO_2 is more favorable for its adsorption on Ni111. In this study, the adsorption energies were calculated using SIESTA and the results were tuned up using van der Waal counterpoise correction. Four different sites

and orientations were selected to study the adsorption and know the most active site among them. To produce syngas from DRM, there are a lot of transitional molecules that need to be studied to determine the rate-determining step and these molecules affect the pathway of the reaction. This study shows that carbon can be adsorbed on the surface and that limits the active sites and deactivating the catalyst.

This study has found that Ni-based catalysts can be considered as the optimum metals to be used in DRM among the transition metals. Noble metals were not considered due to their lack of economic feasibility even though they give more favorable results.

Acknowledgments

I would like to thank Prof. Mert Atilhan my first supervisor who I start my thesis with and I appreciate his support and advice especially during the early stages to overcome a lot of obstacles. I would like to thank Prof. Santiago Aparicio Martinez for dedicating his time and utilities to make this study possible and also, for guiding me during different stages of this thesis.

I would like to extend my thanks to Prof. Majeda Khraisheh and Dr. Mohammed Ali Saleh for their support and encouragement to complete this thesis. I appreciate the feedback from them and their patient to complete this study.

Finally, I would like to thank everyone who helped me during my master studies and supported me in anyway. Special thanks to my family who have been always of great believers and advice.

Table of Contents

List of Figures

List of Tables

Chapter1 Introduction

Carbon dioxide CO_2 is one of the main greenhouse gases (GHG) and it is produced mainly as a side product of hydrocarbons combustion. The amount of CO_2 in atmosphere has a direct correlation with the global warming phenomena[1]. It also, increased rapidly in the last few decades globally due to the growing in the industrial applications. In figure.1, it can be seen clearly the increasing level of CO_2 was rapidly till it reached the highest level ever. This has a direct relationship with the combustion of fossil fuel in industrial activities and transport.

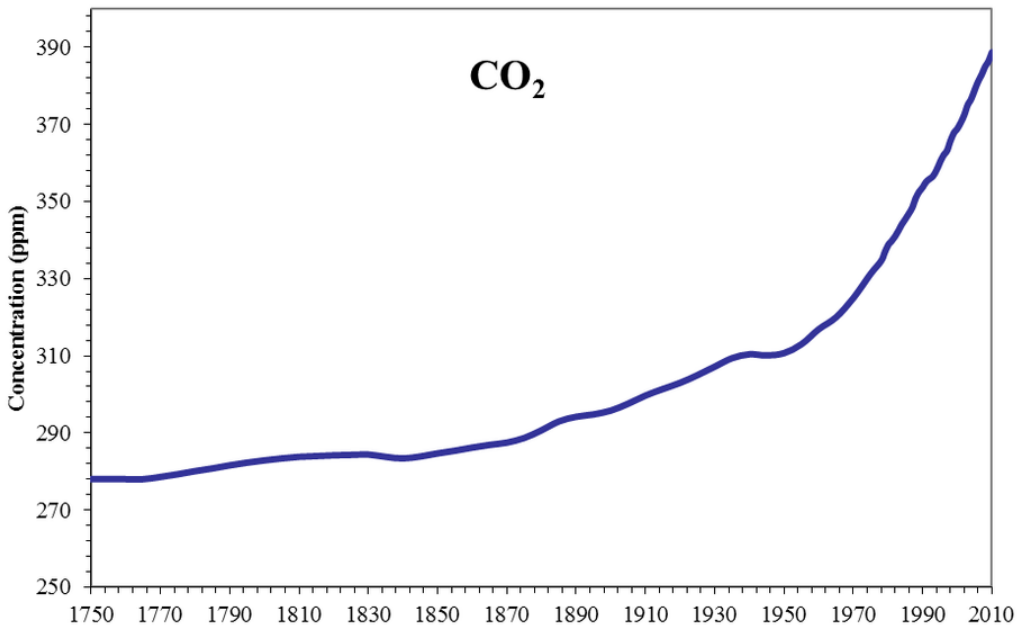

Figure 1: CO_2 Concentration Over Years[2]

Even though, CO_2 is the major GHG, but they are many other gases that play the same role. Figure.2 shows total global GHG that was emitted between the periods of 1751-2010. It also, proves that this increasing level is due to human activities.

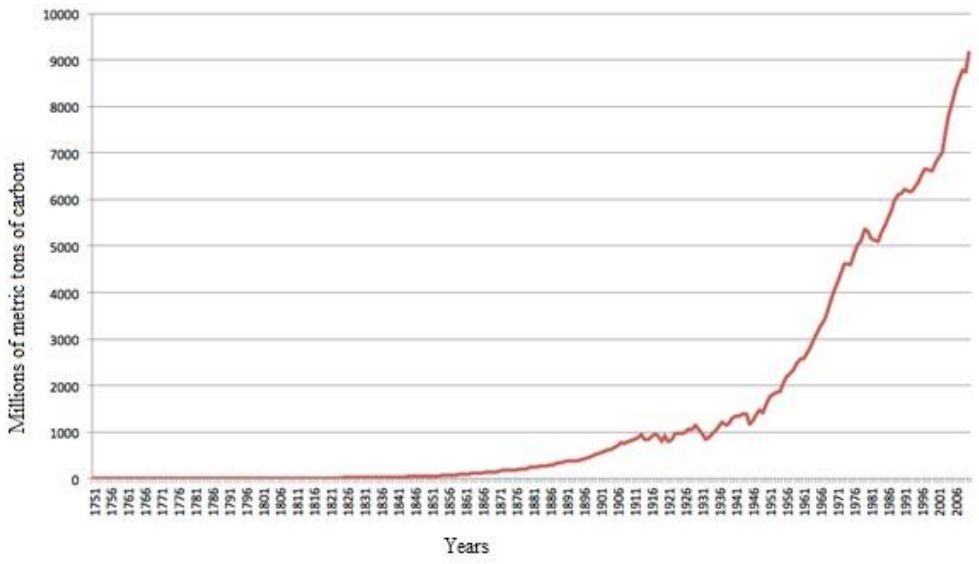

Figure 2: Global GHG Emission per Year (1751-2010) in Metric Tons of Carbon[3]

Earth increasing temperature has catastrophic effects on environment and that could be caused by phenomena such as desertification, melting of ice caps, storms, forest fires and many more. Therefore, the demand of more power production due to the

technological development for the improvement of life style is increasing worldwide which in turn enhances the usage of fossil fuels and subsequently rising CO_2 emission and concentration in the environment [4-6]. The renewal energy sources such as solar power, wind power, nuclear power and bio fuel power are still in the research and initial stages and consequently the world will have to depend mostly on fossil fuels for next few decades. It has been estimated that on average a single power plant using fossil fuels as power production source emits at least 3.5 million tons of CO_2 per year, whereas the number of such power generation industries increases globally[7]. Cement industries and transportation, which are the second and third major sources of CO_2 emission and environment pollution are also multiplying every year and accordingly enhancing the concentration of CO_2 in atmosphere[8]. Research has shown that the content of CO_2 in atmosphere may exceed 500 ppm by 2020 if not handle properly [9, 10]. This alarming increase in CO_2 emission has severely threatened life on the earth and issues like global warming, severe weather conditions spread of very dangerous disease such as respiratory illnesses and asthma are all due to the excessive and uncontrollable emission of CO_2 [11-16].

Focusing on Qatar, the highest CO_2 emission producer per capita, the industrial processing of natural gas is the main source for the greenhouse gases and very small portion is due to the municipal waste burial. Therefore, it is essential to utilize GHG specially CO_2 by capturing and reforming.

1.1 Carbon Capture and Storage (CCS)

The emission of CO_2 can be reduced by introducing capturing and reforming CO_2 units to the process. These units not only can reduce the amount of released CO_2 but it has a financial feasibility as well. There are many technologies that are introduced recently to capture, store and reform the CO_2 and due to CO_2 industrial applications, the need of capturing it has increased. There are many technologies that are used to capture CO_2, storage and further using in industrial applications.

CCS is a technique that is used to capture up to 90% of carbon dioxide emissions. This technology mainly used to capture CO_2 from the combustion of fossil fuels and power generation. The main objective is to prevent the emissions from reaching the atmosphere[8]. The CCS technology consists of three main sections; capturing the CO_2, transport it and storing it in safe conditions. In order to capture the carbon dioxide from the combustion gases, it has to be separated first. This can be obtained in a three ways which are; pre-combustion[17], post combustion and oxy-fuel combustion[18]:

1.1.1 **Pre-combustion:** involves converting the fuel into a mixture of hydrogen and carbon dioxide by different processes, reforming for example and the process is represented in figure.3.

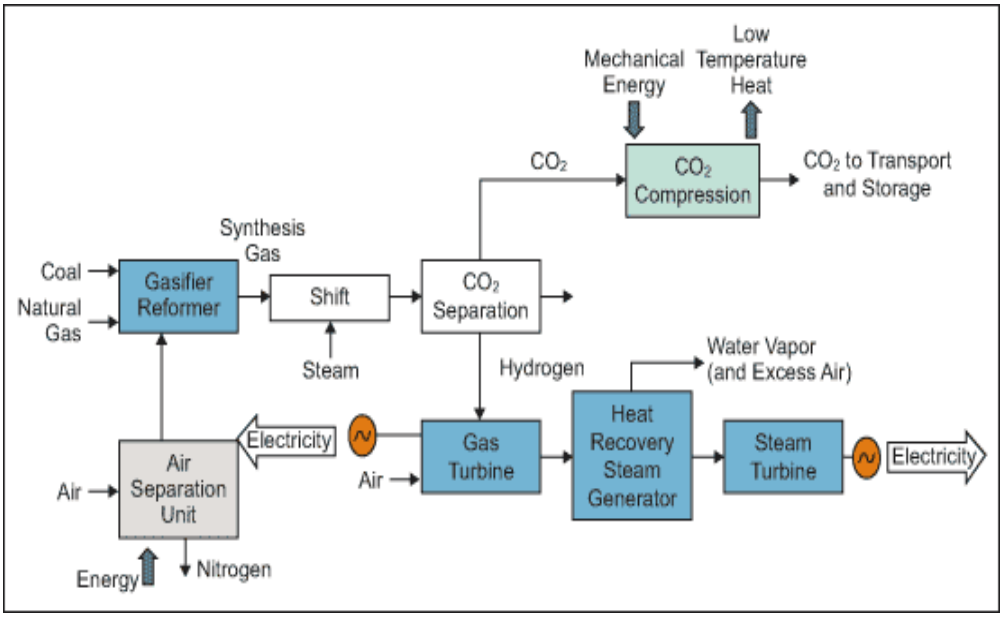

Figure 3: A Pre-combustion Capture System[19].

Air is fed to an air separation unit to separate oxygen from the air. This pure oxygen will react with fuel in a gasifier to produce a syngas. Steam is added to a shift reactor to transform CO to CO_2 and H_2. The CO_2 is captured from the steam. Then, CO_2 will

be compressed and dehydrated in order to transport and store. Hydrogen is combusted to produce electricity and reduce the fuel used in the process.

1.1.2 **Post-combustion:** after combusting the fuel, CO_2 can be captured from the flue gas by using a suitable solvent. The absorbed CO_2 can be liberated from the solvent and then transported to be stored safely and figure.4 illustrates it.

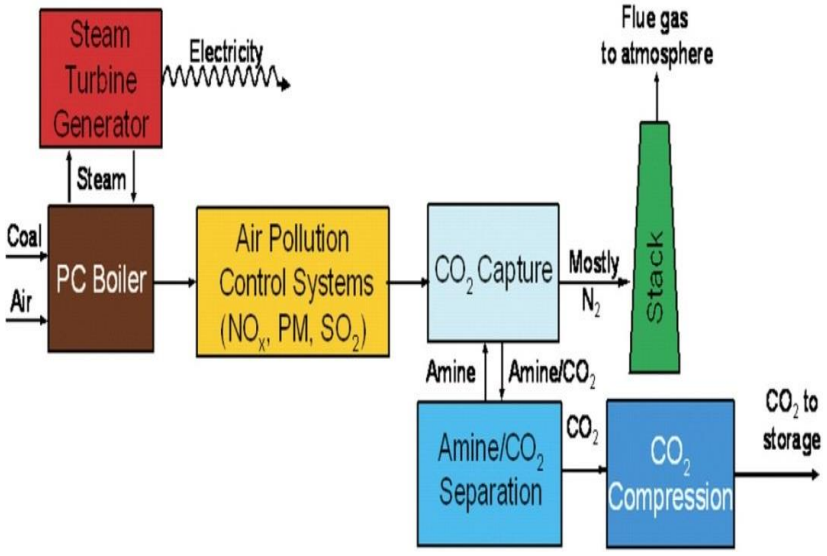

Figure 4: Post Combustion Scheme[20].

Fuel is injected in a boiler and combusted with air. This produce steam to run the turbines and flue gas mainly CO_2, nitrogen and water. The flue gas will pass through a chemical was that separates CO_2. The captured CO_2 will be compressed and dehydrated and ready to transport and storage.

1.1.3 **Oxy-fuel combustion:** by using pure oxygen with recycled flue-gas to combust the fuel as it illustrated in figure.5. The flue-gases from this combustion are mainly CO_2 and H_2O. It makes the separation much easier.

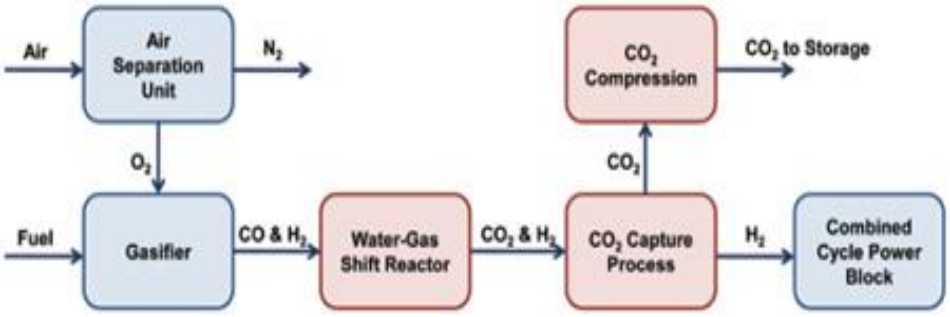

Figure 5: Oxy-fuel System to Capture CO_2[21].

Oxy-fuel combustion burns fuel in pure oxygen instead of air. Air separation unit is used to separate oxygen from air. This pure oxygen will be injected in a boiler with fuel in order for combustion to take place. Steam is generated from the boiler and used to run turbines to generate electricity. Some of the flue gas is recycled to cool down and maintain the boiler temperature. The flue gas is mainly carbon dioxide and water. The carbon dioxide is dehydrated and compressed ready to transport and storage.

Other than above-mentioned three well-known methods there is also another alternative that captures CO_2 via biological methods. CO_2 is captured by using algae and utilizing the solar radiation as energy source. The carbon dioxide capturing efficiency may reach 90% in some reported results [22, 23]. The captured CO_2 is used to produce biomass and biofuel. It's one of the sustainable ways to reduce greenhouse gases.

In recent years, there was an increasing in capital invested in development of microalgae to obtain and enhance biofuels. Microalgae have a higher yield and availability comparing with terrestrial crops. The microalgae capture CO_2 as bicarbonate in ponds, reduce the atmospheric CO_2 emissions. It also reduces the area required to grow the plants. Microalgae produce up to tenfold more biomass than the terrestrial systems due to their high photosynthetic efficiency and figure.6 shows the process.

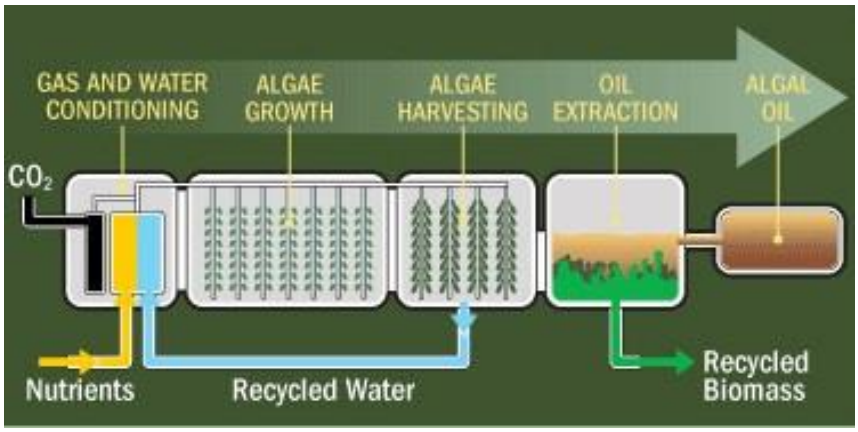

Figure 6: A Bioreactor System to Capture CO_2[24].

Algae based systems can recycle carbon dioxide emissions from industries and it is considered as the most promising solution for emitted CO_2. Algae can capture CO_2 in ponds as bicarbonate to enhance the algal growth. It can be harvested daily despite the seasons. Oil can be extracted from algae to produce fuel. This fuel has high energy content. Algae can be recycled up to 30% and the rest is fermented for methane to be used in power generation.

1.2 Dry Reforming

In order to reduce CO_2 levels, capturing, separating and storing safely are required to be done in economic feasible way. The cost (capital or operational) of these processes must be at the minimum. CO_2 emissions are the main challenge for any manufacturing facility that uses hydrocarbons. Using only captured carbon in CO_2 market is not the answer for this problem as there will be around 99.2% unaccounted for. This shows the difference between the produced and utilized amount of CO_2. The only industry that could effectively requires such sheer volume of output is fuel production. Fuel production from CO_2 has two main problems. First is the economic feasibility as it cost a lot of money and time. Second is related to the technology and the overall goal as recycling all CO_2 from fuel combustion into more fuels, meaning using carbon as energy carrier [25]. More questions will be brought about whether there is a better energy platform than carbon.

However, this maybe the best way to convert CO_2 into less harmful compound to environment and tackle the global warming effects due to the increasing levels of

CO_2. Converting CO_2 safely could be obtained by either redox chemistry (e.g. photosynthesis) or redox free chemistry (e.g. oceanic sedimentation). In photosynthesis, CO2 is reduced into alcohol and aldehydes by photons that are used to activate water. In oceanic sedimentation, $CaCO_3$ is formed. Both pathways are important and they lead to understanding that in order to tackle CO_2, many alternatives should be taken into consideration. Redox chemistry for a CO_2 is more favored as the formation of $CaCO_3$ is slow and not sufficient enough for large-scale operations [2]. The reductive conversions are more costly due to the need of finding electrons to reduce CO_2.

In contrast, dry reforming of methane (DRM) is a process that can reduce CH_4 and CO_2 into syngas and it takes into account the economic feasibility. The main feature of DRM is represented as following [26, 27]:

$$CH_4 + CO_2 \leftrightarrow 2CO + 2H_2 \quad \Delta H_{298} = 247 \ \frac{kJ}{mol} \qquad \text{(Eq.1)}$$

This process utilizes two of the greenhouse gases to produce syngas that is used as a feedstock to many industrial applications such as methanol synthesis. In Qatar, there is a mega methanol plant which is using steam reforming on CH4 in order to produce syngas. This process is highly endothermic and faces a lot of operational and environmental challenges. The produced methanol in Qatar is used to produce methyl tert-butyl ether. In methanol synthesis, reducing the operating cost can be done by decreasing temperature and increasing the pressure.

Although, DRM is still under continuous researching, it shows a lot progress on overcoming the main challenges to commercialize this process. However, tackling these problems is not easy due to many factors such as; cost of applying these technologies and overcoming operational challenges which is mainly carbon formation and deposition on the catalyst[28]. DRM and steam reforming of CH4 are both highly endothermic conversion to produce syngas and they both require a catalyst to reduce the energy input [29-31]. The Shell Pearl GTL plant in Qatar is the largest GTL plant that uses partial oxidation (POX) technology in order to produce syngas which is need for their Fisher-Trophs synthesis (FTS) plant. The plant is located in north of Qatar where most of the natural gas production takes place and it is known that Qatar is one of the largest natural gas producers globally. Oryx GTL plant is another plant that produces syngas in Qatar and it uses auto-thermal reforming technology (ATR) which is a combination of the endothermic steam reforming (SMR) and the exothermic partial oxidation.

The previously mentioned technologies show that it is a design option as they can produce high-quality and high H_2/CO ratio syngas that is higher than the required for FTS (H_2/CO>2). SMR produces syngas with a ratio H_2/CO ratio 3:1 which is lower than many industrial applications that can produce up to 5:1 based on CH_4 conversion, however, SMR is energy intensive [32]. POX is exothermic commercial technology that produces syngas with H2/CO ratio around 2 and it does not need a catalyst. However, POX requires air separation unit which is more cost and may reach up 65% of the utilities costs of the overall GTL plant cost. Moreover, POX is

highly exothermic and that is associated with many concerns related to the safety of the process due to the hotspots and runaway reactions [33].

On the other hands, DRM produces a syngas with H2/CO around 1:1 which is CO-rich [32]. Commercializing DRM has faced a lot of obstacles such as the need of concentrated CO2 to be supplied and the high energy input which about 50% higher than SMR is. Catalyst deactivation due to carbon deposition and low H2 syngas content are more obstacles to be faced [32-34]. Therefore, DRM commercialization has been limited to small sized plant such as CALCOR [35] and SPRAG [36] despite its potentials for producing synthetic fuel while mitigating CO_2. Nevertheless, DRM is a promising technology that reform CH_4 by utilizing a large amount of CO_2 and H_2 is not limiting syngas further processing [29, 31].

In this technology, different metals and different surfaces have been studied and tested in order to come-up with optimum catalyst. In this thesis, screening of different Ni surfaces and alloys is used to choose a metal that maybe yield the best possible reforming results. There are few criteria that are considered while approaching this selection such as availability, cost of production and resistivity of carbon formation and deposition on the surface of the catalyst.

Based on these criteria, transition and noble metals are more likely to be used and to choose the right metal among them [37-43]. Transition metals have high densities, high melting points, easy to shape and variable oxidation states. Also, they form stable complexes that can be used as base to enhance targeted properties. High

melting points of transition metals which are an essential for the stability of any catalyst that operates in high temperature medium. Noble metals were excluded because they are expensive and limited availability even though they are more stable and high conversion rate[44]. Therefore, transition metals can be considered as the more optimum choice[45]. The disadvantage of using transition metals is the coke formation and fast deactivation [42, 46, 47]. Other factors are used in screening metals to choose among them such as rate of reaction, activation energy and adsorption energy. To evaluate these factors, in the following section there will be comparing tables that justify selecting of the metal.

1.3 Kinetics

In the last few decades, there were many approaches to study CO_2 dissociation and interaction with the transition metals[42]. These approaches concluded that the CO_2 dissociation on transition metals is possible and it varies from a metal to another. The CO_2 dissociation is represented as the following [48-50]:

$$CO_2(g) = CO^* + O^* \qquad \text{(Eq.2)}$$

$$CO^* = CO + * \qquad \text{(Eq.3)}$$

In figure.7, it shows the dissociation of CH_4 and CO_2 of DRM.

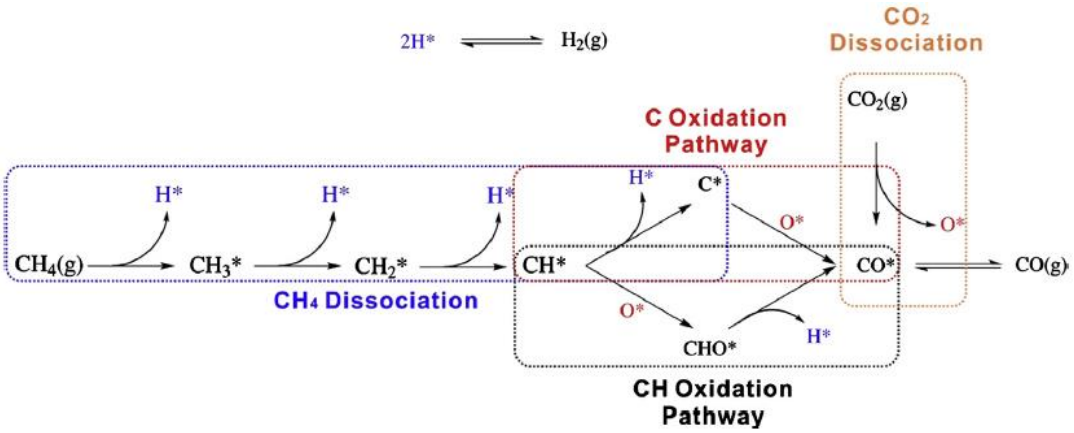

Figure 7: Dominant Reactions Pathway of DRM[47].

The dissociation of methane is another major mechanism that has to be studied in order to get a better understanding of dry reforming. The methane dissociation undergoes the following main reactions [27, 34, 47, 51-57]:

$$CH_4(g) + 2^* \rightarrow CH_3^* + H^* \quad \text{(Eq.4)}$$

$$CH_3^* + * \rightarrow CH_2^* + H^* \quad \text{(Eq.5)}$$

$$CH_2^* + * \rightarrow CH^* + H^* \quad \text{(eq.6)}$$

$$CH^* + * \rightarrow C^* + H^* \quad \text{(Eq.7)}$$

$$C^* + O^* \rightarrow CO^* + * \quad \text{(Eq.8)}$$

$$CH^* + O^* \rightarrow CHO^* + * \quad \text{(Eq.9)}$$

$$CHO^* + * \rightarrow CO^* + H^* \quad \text{(Eq.10)}$$

$$CH_2^* + O^* \rightarrow CH_2O^* + * \quad \text{(Eq.11)}$$

1.4 Carbon Deposition

Carbon deposition is one of the main challenges that are facing the dry reforming process. Carbon generated from the reaction within the process will reduce the number of the active sites on the catalysts.

Considering Ni-based catalysts, there are two types of carbon deposited are observed [37, 38, 41, 57, 58]:

- Carbon from the feed (CO_2 and CH_4) dissociation. This type is stable and blocks the active sites.
- Carbon alloyed with Ni such as Nickel carbide.

Moreover, Ni flat surfaces are found to have higher activation energy and higher resistance to coke formation [47]. After performing kinetic analysis, it is reasonable to say that coke formation is controlled by two properties:

- The extent of CH oxidation pathway in overall CH_4 dissociation.
- The barrier energy of CO dissociation in overall CO_2 dissociation.

There are two side reactions that generate carbon and lead to catalyst deactivation [42, 45, 59-61].

$$2CO \rightarrow CO_2 + C \qquad \Delta H_{298K} = -171 \frac{kJ}{mol} \qquad \text{(Eq.21)}$$

$$CH_4 \rightarrow 2H_2 + C \qquad \Delta H_{298K} = 75 \frac{kJ}{mol} \qquad \text{(Eq.22)}$$

In order to enhance the catalyst for dry reforming, it is recommended to have better coke formation resistance by adding elements such as Al, Fe, Ce and Mg since the coke formation is a major challenge for this process and it increase the operational cost which makes it add obstacle for commercializing [38, 40-42, 44, 47, 61-63]. Among Ni and Ni-based catalysts, Ni111 has the lowest coke deposition on its surface which means that the coke formation and deposition on the surface is slow [47]. The resistance of coke formation on Ni111 could be for two properties: First, the CH oxidation is preferred on Ni111 which leads to slower coke formation from methane. Second, the CO dissociation activation energy is 3 eV which is considered to be high [26, 47].

1.5 Rate of Reactions

The overall reactions rates on Ni and Ni-based catalysts were calculated in order to determine the most active surface among them for dry reforming process and represented in table.1 [47, 54]. Based on these calculations, Ni111 with overall rate of 23.49 s^{-1} is the most active surface among them. The overall reaction rates were 3.86 s^{-1}, 0.48 s^{-1} and 0.44 s^{-1} for the surfaces Ni_3C (001), Ni (211) and Ni_3C (111), respectively. The overall reactions were calculated at 1000 K and 0.1 bar [47].

Table 1: Rate of Reaction on Different Metal Surfaces [47, 54]

Catalyst	Ni111	Ni211	Ni3C(001)	Ni3C(111)
r overall	23.49	0.48	3.86	0.44
r C	0.22	0.23	0.25	0.31
r CH	23.26	0.25	3.61	0.13
Θ	0.62	0.01	0.02	0.01
Θ CO	0.31	6.87E-03	0.13	0.07
Θ H	0.05	1.00E-03	0.01	2.86E-03
Θ O	3.16E-03	1.37E-04	0.01	5.35E-03
Θ C	4.40E-04	9.80E-01	0.32	0.85
Θ CH	0.01	2.51E-03	0.52	0.06
Θ CH2	3.10E-05	1.25E-07	4.41E-04	5.61E-06
Θ CH3	3.46E-06	1.58E-07	6.84E-06	8.58E-07
Θ CHO	7.82E-09	2.07E-09	1.97E-09	2.36E-08

The simulations were on micro-scale and they have been used to quantify and determine the activity of DRM and the overall reaction rates. Following in table 2 are the formulas that have been used to calculate the overall reaction rates. Each step's reaction rate is equivalent to the forward reaction minus reversed reaction.

Table 2: Overall Rate Reaction of Dry Reforming Process [47, 64, 65]

Step *i*	Reaction elementary step	Rate equations
1	$CO_2 + 2^* \leftrightarrow CO^* + O^*$	$r_1 = k_1 P_{CO}/P^o\theta_*^2 - k_{-1}\theta_{CO}\theta_O$
2	$CH_4 + 2^* \leftrightarrow CH_3^* + H^*$	$r_2 = k_2 P_{CH4}/P^o\theta_*^2 - k_{-2}\theta_{CH3}\theta_H$
3	$CH_3^* + * \leftrightarrow CH_2^* + H^*$	$r_3 = k_3\theta_{CH3}\theta_* - k_{-3}\theta_{CH2}\theta_H$
4	$CH_2^* + * \leftrightarrow CH^* + H^*$	$r_4 = k_4\theta_{CH2}\theta_* - k_{-4}\theta_{CH}\theta_H$
5	$CH^* + * \leftrightarrow C^* + H^*$	$r_5 = k_5\theta_{CH}\theta_* - k_{-5}\theta_C\theta_H$
6	$C^* + O^* \leftrightarrow CO^* + *$	$r_6 = k_6\theta_C\theta_O - k_{-6}\theta_{CO}\theta_*$
7	$CH^* + O^* \leftrightarrow CHO^* + *$	$r_7 = k_7\theta_{CH}\theta_O - k_{-7}\theta_{CHO}\theta_*$
8	$CHO^* + * \leftrightarrow CO^* + H^*$	$r_8 = k_8\theta_{CHO}\theta_* - k_{-8}\theta_{CO}\theta_H$

By studying different transition metals it can be said that the values are closed from the literature. It can be observed that hydrogen's activation energy is a bit higher than the activation energy of CO formation. The reason could be the occurrence of reversed water-gas reaction that consumes hydrogen and generates CO. Table.4 illustrates activation energies in same direction and it can be observed that the values vary between 2-4 kcal/mol [29, 44, 46, 50, 55, 66-69]. The effect of temperature should be taken into consideration in order to obtain more accurate values.

Table 3: Rates of Reaction for Rh and Pt Based Catalysts

Catalyst	Rate of reaction (s^{-1})			
	rCH4	rCO_2	rCO	rH_2
Rh(0.6%)/La2O3	12.74	13.04	14.18	18.94
Rh(1.0%)/Al2O3	-	-	16.00	18.00
Rh (1.0%)/MgO	-	-	20.00	23.00
Rh (1.0%)/TiO2	-	-	12.00	16.00
Rh(3.8%)/SiO2	19.00	21.73	20.77	23.40
Pt(0.83%)/ZrO2	18.40	15.00	15.00	16.80
Pt(0.86%)/Al2O3	22.50	20.20	18.50	19.30
Pt(0.31%)/ZrO2	24.00	20.00	21.60	34.00
Pt(0.82%)/TiO2	23.00	19.00	20.50	32.00
Pt(0.75%)/Cr2O3	16.00	15.00	16.00	19.00

The previous results were obtained using ab initio computational approach using VASP coding and they are in compliance with the experimental data. The model was used to understand the favored pathways of the dry reforming reactions and to determine the rate determining step. The main two pathways in this reaction network are: CH_4 dehydrogenation and CO_2 dissociation. The detailed reaction network is not accessible experimentally and therefore simulation models are used to predict these pathways [67].

1.6 Adsorption Energy

Adsorption energy is the main parameter that this study is focusing on and it will be discussed in details later on. The physisorption of CO_2 on transition metals' surfaces is calculated to be around 0.3 eV regardless the type of the catalysts and its actives where the physisorption takes place as table.4 represents the adsorption energy [22, 70]. CO_2 cannot be chemisorbed on metallic planes that are low-indexed especially for copper comparing to the other metals. Chemisorption of CO_2* could not be measured for Ag (111), Cu (111) and Au (111) and they have been studied to come up with a general trend for transition metals [38, 48, 71-74]. The overall CO_2 dissociation reaction rate is governed by the following reaction among many other pathways [26, 38, 49, 75, 76]: $CO_2 \rightarrow CO + O$ (Eq.23)

Table 4: Adsorption Energies for CO_2 on Different Catalysts

Catalyst	E_{ads} CO_2 (eV)	E_{ads} CO_2* (eV)
Fe(110)	-0.24	-0.93
Ir(111)	-0.34	-0.35
Ru(0001)	-0.32	-0.65
Pd(111)	-0.33	-0.18
Rh(111)	-0.33	-0.36
Ni(111)	-0.27	-0.21
Pt(111)	-0.22	-0.03
Co(0001)	-0.26	-0.31
Cu(111)	-0.24	0.23
Ag(111)	-0.26	0.28
Au(111)	-0.3	0.42

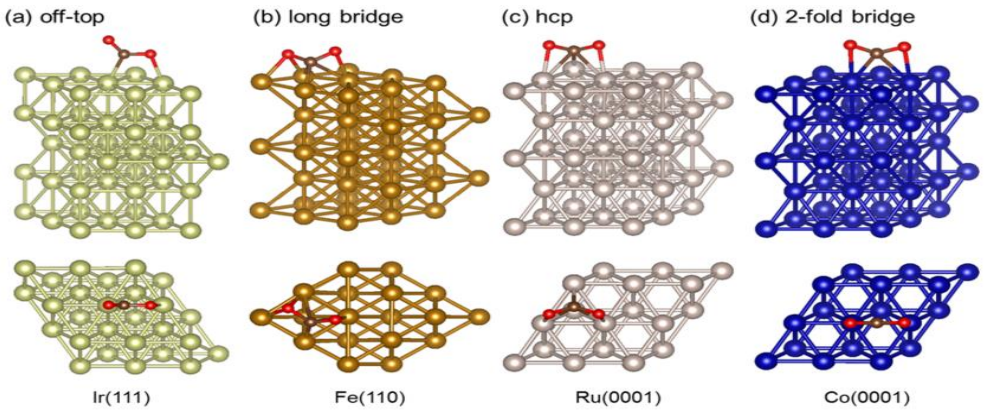

Figure 8: Optimized Geometries of Adsorbed CO* at Ir(111), Fe(110), Ru(0001) and Co(0001) Surfaces[38, 48, 71-74]

There is a relationship between the chemisorption of CO_2 and the metal's surface of the transition metal. CO_2 chemisorption on the metal's surface is due to the charge transferring from the surface with the bending structure (Figure 8) which is known as density of state and vibrational frequency [77-79]. The stability of the metal surface (111) can be arranged as: (Ni, Ir, Cu, Pd, Pt, Rh, Ag and Au) [44, 46, 50, 55, 67, 68]. CH_4 dissociation contains four dehydrogenation reactions steps, while CO_2 dissociation contains one step. The chemisorption has been calculated using the following [47]:

$$\Delta E_{ads} = E_{adsorbate-surface} - E_{adsorbate} - E_{surface} \quad \text{(Eq.24)}$$

The negative value means a stronger binding energy between the adsorbate and the surface. The adsorption energies were calculated on the most favored active sites and were summarized in table.5 [10, 13, 20, 28]:

Table 5: Adsorption Energies of Reactants and Intermediate Molecules

Catalyst Species	Ni111	Ni100	Ni211	Ni3C(001)	Ni3C(111)	Pd	Pt
				E_{ads} (eV)			
CH3*	-1.91	-1.87	-2.17	-2.27	-2.28	-1.95	-2.1
CH2*	-4.01	-4.32	-4.06	-4.41	-4.28	-4.92	-4
CH*	-6.35	-7.06	-6.67	-6.69	-6.76	-6.65	-6.7
C*	-6.85	-8.22	-7.95	-7.3	-7.69	-6.95	-6.88
O*	-5.72	-5.98	-5.9	-6.22	-6.11	-4.8	-4.35
CO*	-1.94	-1.95	-1.97	-2.18	-2.15	-2.3	-1.55
CHO*	-2.27	-2.85	-2.58	-2.61	-2.69	NA	NA
H*	-2.8	-2.75	-2.84	-3.1	-2.98	-2.88	-2.71

Several features can be identified from the chemisorption energies that are listed above. Firstly, for all the adsorbed species, the binding energies on Ni111 are the weakest among them all. Secondly, Ni3C(001) shows the strongest binding with every adsorbate., except for CHO, CH and C species due to the active site influence, which tend to bond powerfully with high valence adsorbates [27, 47].

1.7 Activation Energy

It is the minimum energy required for reactant species to have in order to transform them into products. This energy differs from a metal to another and the following table compares between Ni111, Lanthanum Zirconate Pyrochlores LRhZ (011) and LRhZ (111) that are used in dry reforming of methane DRM [40, 54, 55, 64, 67, 80-82]

Table 6: Activation Energy for DRR on Ni111, LRhZ(011) and LRhZ(111)

	Ni111		LRhZ(011)		LRhZ(111)	
Reaction	$E_{a,f}$ (eV)	$E_{a.r}$ (eV)	$E_{a,f}$ (eV)	$E_{a.r}$ (eV)	$E_{a,f}$ (eV)	$E_{a.r}$ (eV)
$CH_{4(g)} + * \rightarrow CH_4^*$	0.00	0.02	0.00	0.13	0.00	0.07
$CH_4^* \rightarrow CH_3* + H*$	0.91	0.90	0.38	1.75	0.89	1.46
$CH_3* \rightarrow CH_2* + H*$	0.70	0.63	1.41	2.80	0.81	1.07
$CH_2* \rightarrow CH* + H*$	0.35	0.69	2.70	3.86	2.53	3.28
$CH* \rightarrow C* + H*$	1.33	0.81	3.74	3.18	3.37	2.71
$CO_{2(g)} + * \rightarrow CO_2*$	0.00	0.02	0.00	2.93	0.00	1.46
$CO_2* \rightarrow CO* + O*$	0.67	1.65	3.63	1.31	2.53	1.26
$CO_2*+H* \rightarrow COOH*$	1.13	0.85	0.22	3.59	1.47	0.74
$COOH* \rightarrow CO* + OH*$	0.57	1.65	0.22	3.59	0.10	1.65
$CH_3* + OH* \rightarrow CH_3OH*$	2.20	1.61	3.15	0.01	2.52	0.01
$CH_3OH* \rightarrow CH_2OH* + H*$	0.88	0.69	0.66	1.79	0.81	1.11

CH_2* + OH* → CH_2OH*	1.32	0.60	3.42	0.01	2.47	0.01
CH_2OH* → CHOH* +H*	0.53	0.90	1.83	1.67	2.12	0.93
CH* + OH* → CHOH*	1.48	0.80	6.43	1.70	4.42	0.01
CHOH* →COH* +H*	0.15	0.86	2.96	5.52	NA	NA
C* + OH* → COH*	1.46	2.01	3.34	1.73	NA	NA
COH* → CO* +H*	0.98	1.97	1.66	3.58	NA	NA
CH_3*+O* → CH_3O*	1.59	1.31	2.57	0.11	2.50	1.05
CH_3O* → CH_2O* +H*	0.93	0.64	2.29	2.88	2.28	1.92
CH_2*+O* → CH_2O*	1.45	0.95	3.49	0.23	2.88	0.80
CH_2O*→ CHO*+H*	0.36	0.74	1.74	3.58	1.37	2.34
CH* +O* → CHO*	1.53	1.08	6.90	4.31	4.01	2.16
CHO* → CO* +H*	0.20	1.48	3.08	3.15	2.40	2.26
C* +O* → CO*	1.59	2.94	5.49	3.54	3.31	1.97
CH_3OH* → CH_3O* +H*	0.89	1.38	1.44	4.39	0.33	1.82
CH_2OH* → CH_2O* +H*	0.63	1.04	0.12	2.53	0.91	1.73
CHOH* → CHO* +H*	0.71	1.14	1.30	5.70	0.01	3.00
O* +H* → OH*	1.35	1.16	5.60	3.34	1.74	1.30
OH* +H* → H_2O*	1.33	0.92	3.04	0.01	2.08	0.01
H_2O*→ $H_2O_{(g)}$	0.29	0.00	0.93	0.00	0.79	0.00
H* +H* → H_2*	0.92	0.06	2.65	0.05	1.16	0.05
H_2*→ $H_{2(g)}$	0.22	0.00	0.19	0.00	0.38	0.00
CO* → $CO_{(g)}$	1.92	0.00	2.53	0.00	1.63	0.00
CH_3OH* → $CH_3OH_{(g)}$	0.30	0.00	0.78	0.00	0.78	0.00

By comparing the activation energies for the above metals, it can be said that Ni111 is the optimum among the three compared catalysts [38, 39, 43, 45, 54, 76, 82-84]. The energy input is the main obstacle when it comes to commercialize dry reforming techniques. Coke resistance is the high on Ni111 surface comparing to other catalysts. Table 7 represents the activation energy of DRM for different Ni-based catalysts [37, 40, 42, 46, 57, 59, 61, 82, 85-88].

Table 7: Activation Energy of DRM on Different Ni-Based Catalysts

Catalyst	Temperature (K)	E_a CH_4	Ea CO_2	E_a H_2	E_a CO
		(kJ/mol)			
Ni/Al2O3	773-973	50.90	56.10		80.50
Ni/Al2O3	673-773	70.60	69.00	98.10	74.00
Ni/SiO2	673-773	62.30	69.80	93.90	68.90
Ni/TiO2	673-923	NA	59.80	NA	NA
Ni/C	673-823	121.40	92.10	134.00	100.50
Ni/MgO	673-823	92.10	87.90	146.50	87.90
Ni/LaO2	923-1023	55.30	NA	NA	NA
LaSrNiO4	633-713	41.80	12.40	NA	NA
Ni/ZrO2	723.00	58.62	41.87	NA	50.24
0.3Pt-10Ni	NA	26.90	23.60	24.90	35.80
0.2Pt-15Ni	NA	26.60	16.90	21.00	35.20

In table 7 it can be observed the temperature on different catalysts and the different alloy on Ni. Adding different metal to Ni it improves the activation energies and lower the amount of energy required for the process [38, 40, 82, 89]. Adding noble metal will reduce the activation energy that is required as it can be observed in the previous table. Noble metals are not feasible when it comes to commercialize DRM. The higher cost of the metal and it stability are the major challenges. Since dry reforming is an endothermic process, the optimum catalyst should require less energy input. Therefore, noble based catalysts are favored from energy saving point of view [90]. Based on the literature review above, Ni111 is a good choice to start the simulation and investigate its properties. It is widely available, low cost and highly resistive to carbon deposition. Also, it shows reasonable adsorption/activation energies.

The main reasons to consider DRM are; producing syngas that can be used in different industries, reducing the amount of greenhouse gases by economic feasibly method. These requested data are important to have a clear understanding of DRM mechanism and pathway. Moreover, it indicates the amount of energy required as input and that reflect the economic feasibility of the whole process. The carbon deposition study dictates the additional utilities for better operating conditions.

1.8 Objectives

As mentioned earlier, the greenhouse gases had increased dramatically in the last few decades. They are emitted mainly from industrial sources by combusting fossil fuels and that is leading to disturb and endanger the ecosystem and human life. It also increases the global warming phenomena. Therefore, researchers are studying different ways to mitigate and reduce the effects of GHG on the environment by studying different technologies that may capture or reform these gases. The main focus in this study is on CO_2 reforming by DRM.

The main objectives of this study are to understand DRM process and its kinetics. More objectives are to study different potential sites and molecular orientations on the catalyst in order to choose the optimum conditions. This can be approached by performing accuracy test using density functional theory. Moreover, this study aims to establish simulation routine for fast calculations for adsorption energies, bond lengths, atomic distance to surface and angles of molecules. In this study, different surfaces of metals will be evaluated and density functional theory (DFT) calculations will be performed on a chosen surface based on selected criteria in the literature review.

Chapter2 Literature Review

2. Density Functional Theory

Density Functional Theory (DFT) is a computational method for quantum mechanical calculations based on modelling approaches. It is used in chemistry, physics and different science to examine the ground state of many-body simulations. It is based on the electron density rather than wave-functions and that is in contrast to HF theory. Electron density is easier to be investigated experimentally using X-ray diffraction. The energy of the system can be described using electron density associated with corrected Hamiltonian operator. There are many theories that can be used in order to carry on this study.

2.1 Functionals

The functionals represent different approximations to exchange-correlation functional

2.1.1 Local Density Approximation (LDA)

LDA is considered to be the simplest and the base of the exchange-correlation functionals. It uses the electron density of a uniform electron gas. LDA was introduced by Kohn and Sham initially and it is given by

$$E_{xc}^{LDA} = \int \rho(r)\epsilon_{xc}(\rho)dr \qquad \text{(Eq.12)}$$

Where ρ is the electron density and $\epsilon_{xc}(\rho)$ is the exchange-correlation energy per particle of uniform electron gas of density and its potential is governed by

$$v_{xc}^{LDA}[\rho(r)] = \frac{\delta E_{xc}^{LDA}}{\delta \rho(r)} = \epsilon_{xc}(\rho) + \rho(r)\frac{\partial \epsilon_{xc}(\rho)}{\partial \rho} \qquad \text{(Eq.13)}$$

Where $v_{xc}^{LDA}$is the exchange-correlation energy density.

Using LDA calculations practically, it is necessary to determine the exchange-correlation for a uniform electron gas of a given density. $\epsilon_{xc}(\rho)$ is split into exchange and correlation potentials as following:

$$\epsilon_{xc}(\rho) = \epsilon_x(\rho) + \epsilon_c(\rho) \qquad \text{(Eq.14)}$$

The exchange potential is given by the Dirac functional:

$$\epsilon_x[\rho(r)] = -\frac{3}{4}\left(\frac{3}{\pi}\right)^{\frac{1}{3}}\rho(r) \qquad \text{(Eq.15)}$$

Accurate values for $\epsilon_c(\rho)$ have been determined from Quantum Monte Carlo (QMC) calculations. These have then been interpolated to provide an analytic form for $\epsilon_c(\rho)$

2.1.2 Generalized Gradient Approximation (GGA)

LDA is a zeroth order approximation and it has low accuracy and to enhance it; generalized gradient approximation was developed. It has the gradient of electron density which shows the non-homogeneity of the real electron density. GGA is divided into exchange and correlation terms and they are solved separately as in the following equation:

$$E_{XC}^{GGA} = E_X^{GGA} + E_C^{GGA} \qquad \text{(Eq.16)}$$

GGA uses non-exhaustive several of efficient GGA functionals to perform computational calculations such as;

P86: Perdew developed a correlation functional that includes an empirical parameter fitted for neon atom.

PW91: this exchange correlation functional was developed by Perdew and then Perdew, Wang and Burke.

PBE: an exchange-correlation functional developed by Perdew, Burke and Ernzerhof.

There are many approaches to perform DFT calculations which deal with spin polarized system, multicomponent system, free energy at finite temperature and many other calculations [27, 50, 91, 92]. The use of these simulations codes will ease the calculations and provide more accuracy. There are many density functional theories can be used but for dry reforming and transition metals, it is recommended to use the general gradient approximation (GGA) [26, 45, 47]. To enhance the accuracy of the simulation, Pardew-Burke-Ernzerhof (PBE) was used. PBE is a van der Waal correlation that takes into account the van der Waal interaction forces and its parameters were obtained from ab-initio calculations[55].

2.2 Quantum Mechanics

Computational methods have been used to study and evaluate the metal's surfaces and perform thermodynamic calculations[78]. In such methods, density functional theory (DFT) is used to perform these calculations and it is considered as one of the

most promising technologies that can compute the electronic structure of a metal [27, 55]. DFT solves the Schrodinger equation with a high accuracy and lower cost; depending on the size of the system that is submitted. The smaller systems are more accurate and faster to give results. Solving the Schrodinger equation could predict the electronic system's behavior. DFT simulations are limited to maximum up to 200 atoms in any simulation; thus the studied system must be well chosen for short-range interaction calculations via DFT techniques.

2.3 Many Body Problem

Many-body problem is a term that is used when there is a big number of interacting molecules on a micro scale to solve systems that are ruled by Schrodinger equation. This concept widely used in quantum mechanics to provide a better accuracy to time-independent non relativistic systems [93, 94]. The Hamiltonian approach is used effectively in colloidal limitation and many-body interaction to allow better improvement in colloidal systems theoretically[94, 95].

2.4 Hartree-Fock Theory (HF)

This theory is based on the molecular orbital theory (MO) which speculates that each electron movement can be described by single particle function. In HF, the Hamiltonian approach could be divided into two parts; a core Hamiltonian part (electron-nuclei) and the electron-electron part. The Hamiltonian equation is as following:

$$H = \sum_i [\, H^c(i) + \sum_{j>i} \frac{1}{r_{ij}}] \text{ with } H^c(i) = -\frac{1}{2}\nabla_i^2 - \sum_A \frac{Z_A}{r_{iA}} \qquad \text{(Eq.17)}$$

2.4.1 Hartree Electron Approximation

The main objective is to approximate the wave function in order to solve Schrodinger equation as a product of single electron wave function [96, 97]. Hartree equations allow researcher to convert 3 Z dimensional Schrodinger equations into a 3 dimensional equation for every electron to be solved by using iteration and variational principle [96, 98, 99]. Since it is non-local and it depends on the spin orbital and due to that it must be solved self-consistently.

The total energy obtained from the solution of the HF approximation is always higher than the real energy. This is due the fact that electrons are considered to be moving in a mediocre electronic field. This implies that the correlated motions of each electron others are omitted. The difference can be represented as following:

$$E_{correlation} = E_{total} - E_{HF} \qquad \text{(Eq.18)}$$

This difference is around 1% of the total energy and it may effects the output of the simulated systems rapidly.

2.5 The Bloch's Theorem

Schrodinger equation solution has a form of $\psi_k = u_k(r)e^{kt}$ (Eq.19)

Where;

- $u_k(r) = u_k(r+T)$ is an amplitude function of the plane wave, exp(ikr) and T are translation of the crystal
- Exp(ikr) multiplied by function uk(r) with the periodicity of the lattice

This type of wave functions is named Bloch theorem function and they are used in DFT calculations where they are very useful. This theorem allows focusing on one period of the lattice to solve wave functions [100, 101].

Chapter3 Technical Approach

Simulations are used to study different types of catalysts and evaluate their activity. DFT calculations can be solved using different coding languages and software such as SIESTA and VASP. They are efficient and provide accurate results. This study compares between SIESTA and VASP as following:

3.1 SIESTA

SIESTA is a combination between a method and its software program to be used in electronic structures calculations by solving DFT equations. The efficiency of this method depends highly on the basis sets that are used and implementation of linear-scale algorithm. The accuracy of the software and its cost has a wide range depending on the required output[102]. Moreover, this method can perform ab initio molecular dynamics simulations of solids and molecules. DFT is used to predict the physical properties of atoms and electron density[103]. The first calculations of DFT are usually performed using SIESTA software based on norm conserving pseudopotentials and numerical atomic orbitals, with the local density approximation [16, 70].

3.2 Vienna Ab Initio Simulation Package (VASP)

VASP is a software and coding language that enable scientists to model atomic scale systems in order to many body problems. VASP gives approximate results for Schrödinger equation [78, 104]. The Schrodinger equation predicts the behavior of electronic systems as it is a wave equation of a wave function.

Schrodinger is known as the first person who wrote partial differential equation that predicts how the quantum systems change with time. The solution of Schrodinger is based on Eigen Values that is devised by Fourier [77, 100, 105]. There are sets of conditions that are used in many simulations as a representation of a larger system using representative volume element. These conditions could be temperature, pressure or electronic structures[106].

The selection of the coding language depends on many factors such as, the size of simulated systems (atoms involved); basis set accuracy and running time. To obtain good results from SIESTA, simulated system shouldn't be more than 200 atoms. Although, SIESTA can operate more atoms but that will be reflecting on the accuracy of output files. VASP is being developed frequently and it is used widely. Also, it has a better accuracy when it comes to large simulation systems. However, VASP isn't the best choice for periodic boundary conditions due to pseudopotentials transport with the planewave basis and the source. In this paper, periodic boundary conditions (illustrated in figure 9)has been used for a simulation system less than 200 atoms and therefore, SIESTA has been used [106, 107].

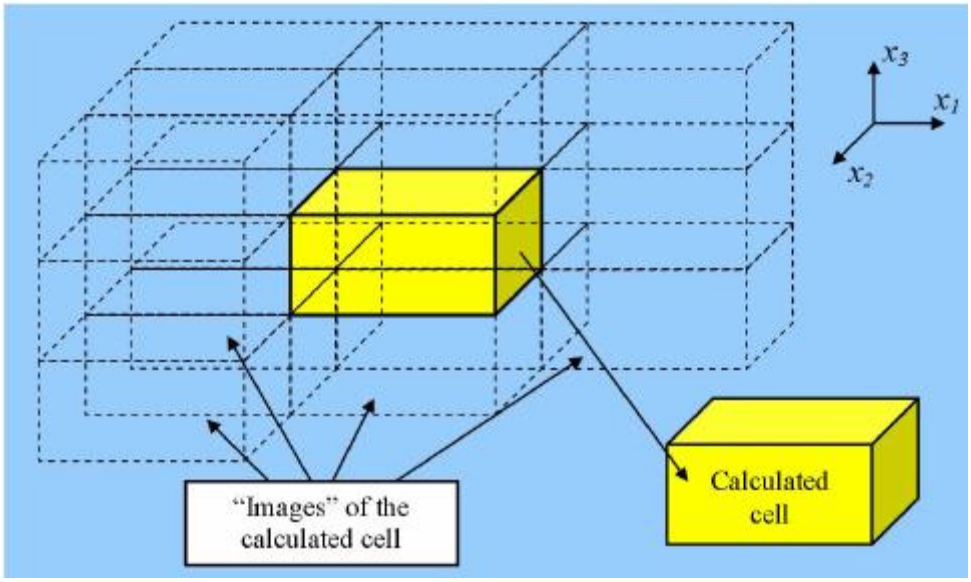

Figure 9: Schematic Representation of The Idea of Periodic Boundary Conditions[108].

Using the two simulation approaches, the binding, activation energies and enthalpy changes were calculated for the following reaction:

$$CO^* + O^* \leftrightarrow CO_2^{**} \qquad \text{(Eq.20)}$$

Table 8: Comparison of Binding Energies (Eads) for CO, Activation Energies (Ea,f) and Enthalpy Changes

Surface	E_{ads} (CO) (eV)			E_a (eV)			ΔH (eV)	
	Experimental	SIESTA	VASP	Experimental	SIESTA	VASP	SIESTA	VASP
Ni111	-1.94	-2.09	-1.88	1.61	1.53	1.60	0.96	1.27
Ni211	-1.97	-2.09	-1.98	1.84	1.57	1.69	0.75	1.00

The differences between the two coding languages are less than 0.1 eV after calculating the activation energy and 0.2 eV in binding energy. These variations are due to the mathematical inaccuracy of the SIESTA solver [54, 109]. In principle, VASP coding and solving is more accurate than SIESTA.

Pseudopotential theory is used to approximate or simplify the complex systems or it is called the effective potential. It is a way to replace the complicated effects of the core electrons and nucleus of an atom. In large systems, it is assumed that the inner electrons are not affected by the surrounding environment [91, 92, 110].

Ab initio method means that a method with no empirical parameters to be used and it is from the first principles. When it comes to DFT, it is a method can be considered ab initio method by practice, especially when using exchange correlations with higher accuracies. Some of these exchange correlations are semi-empirical. LDA and PBE

are considered to be ab initio due to their constraints and can't be fitted. Other exchange correlations functionals such as M06 have parameters that can be fitted. Therefore, it can't be considered to ab initio method [55, 111].

Chapter4 Methodology

In this study, DFT calculations were executed using SIESTA software platform, which utilize Troullier-Martins norm-conserving scalar relativistic pseudopotentials. A double-ζ plus polarization (DZP) basis set was used and it gives fairly well converged results, slightly comparable to the ones used in practice in most plane-wave calculations. This basis sets is a good balance between accuracy and especially computational cost. Generalized gradient approximation (GGA) functional and its Perdew-Burke-Ernzerhof (PBE) form were used in standard DFT supercell approach. GGA functional with a 300 Ry mesh cutoff were used in this study. Spin – polarization of electrons calculations were considered in order to account for the magnetic moment of the catalyst. These calculations considered all forces that effect on the atoms must have a tolerance lower than 0.05 eV/Å. This system has used Ni111, a 2×2 unit cell with five layers and the length to define the scale of the lattice vectors were defined as Lattice Constant 1.0 Ang. The z-direction neighboring cells are separated by a vacuum of ~16.0 Å. Materials Studio was used to prepare the initial structure for coordinates (*.xsd). An input file (Flexible Data Format (fdf)) was prepared for SIESTA simulation and pseudopotentials from Abinit's Fritz-Haber-Institute (FHI) pseudo database data/file. The initial structure was consisting of Ni111 bulk consists of 45 atoms (5 layers). For placing the molecules, it has been taken into consideration the following; horizontal CO_2 molecules are placed 2 A away from the surface and the vertical CO_2 Molecules are placed 3 A from the carbon to the surface.

All distances are measured between the carbon atoms (center of the mass). In SIESTA, 32 cores were used for each simulation.

4.1 The Used Logic

The logic of these simulations factorial design:

- Start with investigating Ni111 surface and its interaction with CO_2 at various locations.
- Orientation of CO_2 molecules at the beginning of the simulations are part of the simulation design.
- Moreover, these simulations considered the active sorption sites and the location of the CO_2 at the beginning of the simulations considering the active sorption sites.
- Start working on PBE-GGA functional and that is based on the outcomes from the literature review.
- Perform counterpoise corrected binding energies at the end to finalize the calculations.
- Same procedure has been used for CH_4.
- Same procedure will be used for selected moleucles such as for CH-, CH_2-, CH_3-, CHOH-, C-, and CH_2OH-.

Counterpoise correction simulations and calculations were performed to obtain corrected adsorption energies as following:

1. E_{NT}: Get final relaxed structure, remove CO_2 and relax again
2. E_{AD}: Get final relaxed structure, remove Ni and relax again
3. $E_{no\text{-}ghost,NT}$: Get optimized final structure, remove CO_2, don't relax the system, just do single point/step calculation (CG=0 in the code)
4. $E_{no\text{-}ghost,AD}$: Same fdf file of step 2 but don't relax the system, just do single point/step calculation (CG=0 in the code)
5. $E_{ghost,NT}$: Single point calculation of the whole system (like step 3) but with CO_2 is ghost molecule (negative terms)
6. $E_{ghost,AD}$: Single point calculation of the whole system (like step 3) but with Ni is ghost molecule (negative terms)

- Initial optimized structure: E_A
- E_{CC} (counterpoise corrected)=$(cp_6 - cp_4) + (cp_5 - cp_3)$
- $E_{AD,CC}$ (counterpoise corrected Adsorption Energy)=$cp_1 + cp_2 – E_A + E_{CC}$

- Once the SIESTA calculations were established and converged, it will be compared the strength of these simulations in comparison with the plane wave basis sets, which are known to work more accurate especially for charge distributions.

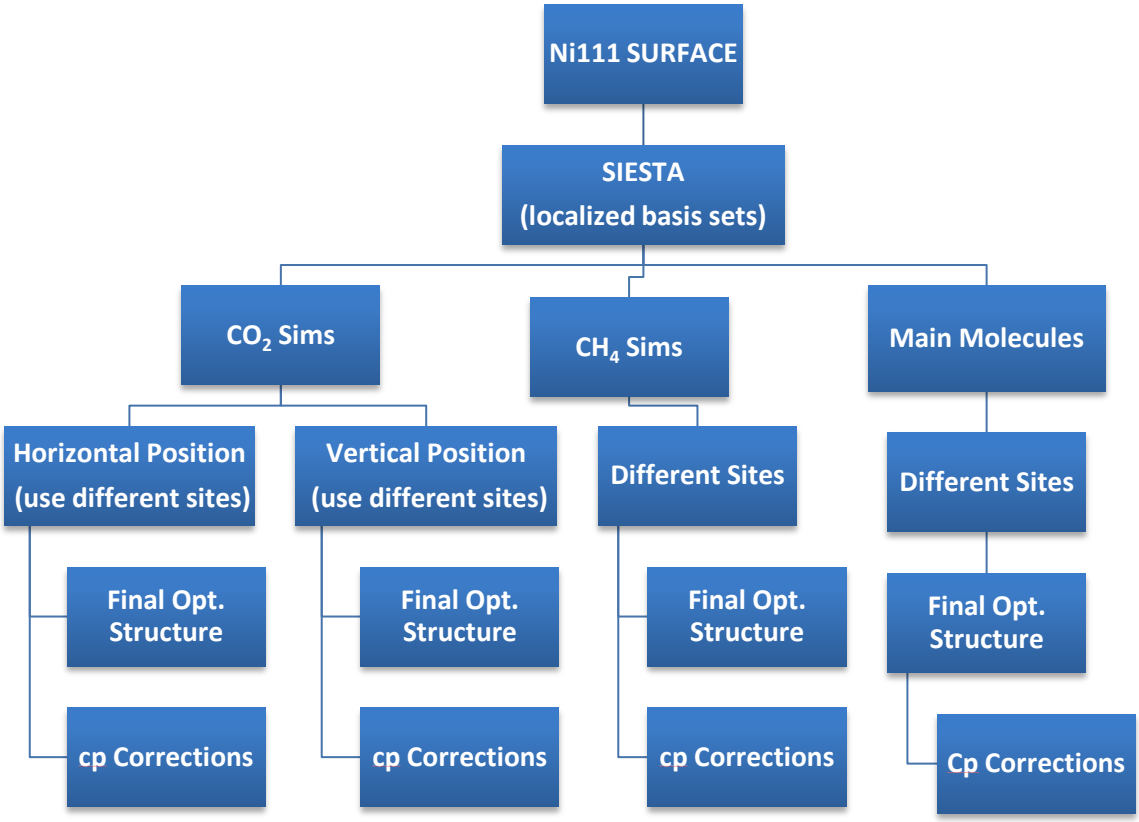

Figure 10: Simulation Organization Used

Chapter5 Results and Discussion

5.1 Geometry

It worth to mention again that SIESTA uses Kohn-Sham self-consistent density functional method in LDA and GGA approximations, as well as non-local functional that includes van der Waals interactions. The output of SIESTA simulation provides a lot of data such as; geometry relaxation, energies (total and partial), atomic forces, electron density and many others [SIESTA Manual]. In this study, the structural information was given directly from fdf files in Cartesians coordinates. In order to optimize the geometry many parameters were used to tune the structure. After introducing the bulk Ni atoms and specifying the lattice parameters, split basis type and DZP size were used for the pseudo-atom-orbitals (PAO). Moreover, dispersion correction using Grimme's method (empirical correction) was introduced to take care of the contribution of van der Waal's forces that are not well described by the functional and basis set that are used in this study. It is essential to have this correction when it comes to the adsorption energies of the system and it has reasonable correction cost. The self-consistent file (SCF) section shows how the program solves the quantum chemistry equations. In this study the tolerance in SCF was set to be 0.001 with max iterations of 300 which were enough for the system to converge (can be edited when it doesn't converge). For optimization of the molecular dynamics (MD) structure, there are many choices but in this study, conjugate gradients (CG) is used to optimize the coordinates as it is the default geometry

optimization method. The other choices are modified Broyden scheme, fast inertial relaxation engine and many others. The default value in SIESTA is CG for structure optimization. It is essential to know that while optimizing the structure, the cell has been fixed as it was defined earlier and only the atoms are subjected to move. Many CG steps are required to reach the minimum energy. The maximum movements of atoms are defined in the fdf file by MD.MaxCGDispl to be 0.8 Bohr.

5.2 CO_2 Interaction

CO_2 molecule is placed horizontally 2 Angstrom from the center of the mass and 3 Angstrom vertically on top of the Ni111 structure that is used in this study. For each orientation, four different sites have been selected to study the adsorption energies and the active sites. From the literature review [27, 47], the adsorption energy of CO_2 molecules on Ni111 is around -0.27 eV. The CO_2 molecule has 180 degree angles between the carbon and oxygen. The change in these angles indicate somewhat of binding energies are affecting the molecule. The typical double bond length between the carbon and oxygen is 1.2 Angstrom and 1.43 Angstrom for the single bond. The following table summarizes the 8 selected sites and their adsorption energies:

Table 9: CO_2 Adsorption Energy of Different Sites

Ni111_1CO_2		
Position	E_{ads} (eV)	Angle ^{o}
H1	0.194	130.74
H2	0.193	131.59
H3	-0.039	131.20
H4	0.102	128.59
V1	-0.234	179.31
V2	-0.036	179.85
V3	-0.219	179.51
V4	-0.260	179.75
	Published	
E_{ads} CO_2 -0.27		E_{ads} CO_2* -0.21

In SIESTA, the sign of the adsorption is defined to be the opposite from the literature. Therefore, when it comes to compare the results, the positive in SIESTA is negative in literature.

The definition in SIESTA [112] is: $E_{ads} = E_{CO2} + E_{surface} - E_{CO2-Surface}$ (Eq.25)

And in the literature is: $E_{ads} = -E_{CO2} - E_{Surface} + E_{CO2-Surface}$ (Eq.26)

To understand the following figures, the atoms are defined by colors as in figure.11.

It can be clearly seen that horizontal orientations gave better results comparing with the literature [27, 47]. The adsorption of horizontal CO_2 molecule was adsorbed on the surface of the Ni forming a bond between the carbon and the surface as illustrated in figure.12. On other horizontal sites, there was a bond between oxygen molecule and the surface was formed. This had a slight effect on the adsorption energy of CO_2. Among the horizontal orientations, the first active site gave the optimum adsorption energy.

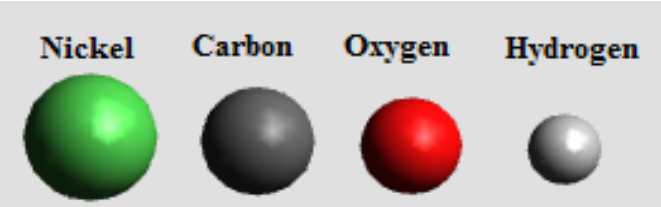

Figure 11: Atoms by Colors

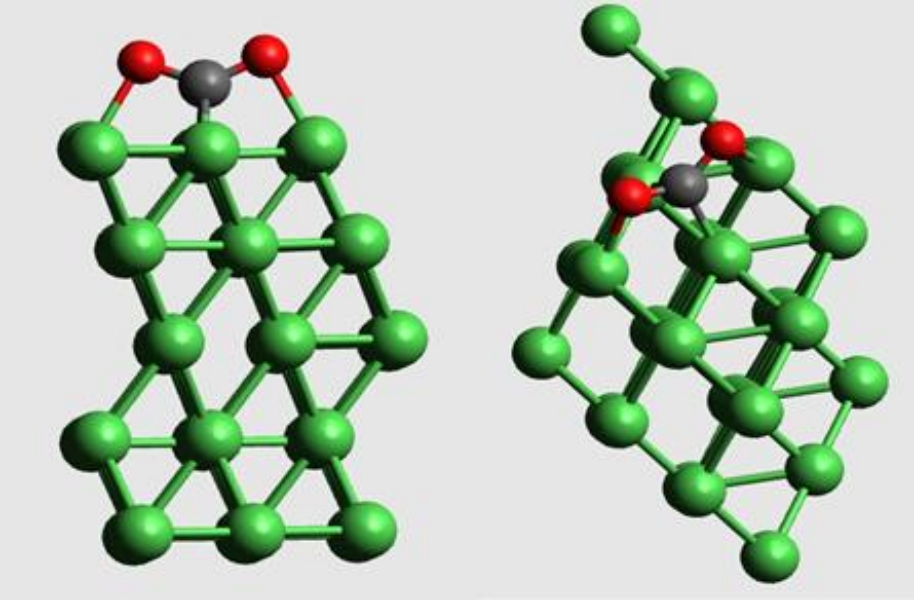

Figure 12: Horizontal CO_2 Adsorption on Ni1111

The four vertical orientations of CO_2 formed different type of adsorption bonding than the horizontal ones. The first two sites formed a bond between the closest oxygen to the surface and the surface. This type of bonding gave non reasonable adsorption energy comparing to literature [27, 47]. The other two sites did not adsorb the CO_2 on the surface. To conclude; horizontal orientations of CO_2 is more favorable active sites and give more reasonable adsorption energies.

5.3 CH_4 Interaction

CH_4 has large C-H bonds, ionization energy and no dipole moment and due to all of these properties, the activation of the first C-H bond in CH_4 is considered to be rate-determining step [47]. It is expected that the CH_4 will be dehydrogenated on the surface of Ni111 in order to reach to the required syngas. In this study, the simulated CH_4 did not adsorbed on the surface as it can be seen in figure 13 and it is believed that the concentration of CH_4 will play a role in dissociation process[27]. Unfortunately, in CH_4 dissociation on Ni111 is considered to be high comparing with the other flat and stepped surfaces of pure Ni and its alloys such as nickel carbide. These other surfaces are found to be around 0.6 eV.

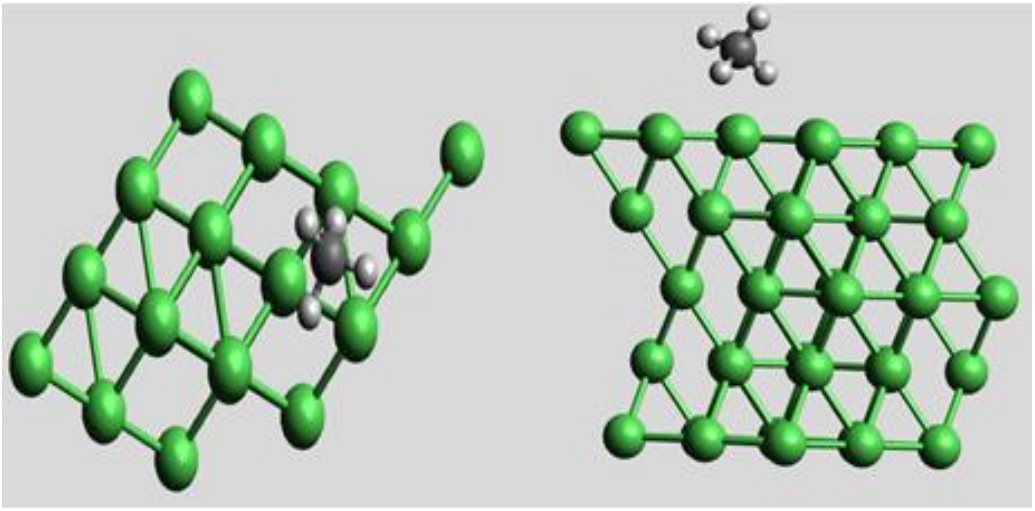

Figure 13: CH_4 Adsorption on Ni111

In this study, the calculated adsorption energies and angles of CH_4 are represented in table 10

Table 10: CH_4 adsorption energies and angles on Ni111

Ni111_1CH_4		
Position	E_{ads} (eV)	Angle
1	-0.148	108.556
2	76.682	110.889
3	0.116	107.988
4	0.185	111.089

These values are lower than ones in the literature [27, 47] and the difference was around 79%. However, due to the properties of CH_4 that are mentioned earlier, the number of layers of both systems plays a major role in this differences.

The regular geometry of CH_4 molecule has a 109^o angles between the carbon and hydrogen atoms and a 1.09 Angstrom bond length. From the previous table, it can be observed that there are forces that are affecting the CH_4 molecules. These forces have changed the angles of CH_4 slightly and could be another indication that this could be the rate-determining step. Among the four selected site, the fourth is most active site.

5.4 Overall Findings

In table 11 there overall system findings (adsorption energies, active sites and angles) are represented and compared to values from literature. These different percentages vary from a molecule to another and they due to different factors will be mentioned while discussing each molecule concerned.

Table 11: Overall Output Simulated System

# sim	Remark	Compound	Eads Sim	Eads Literature [27, 47]	Error %	Angle b/w	Angle
			eV	eV	%	N/A	^{o}
H1		CO_2	0.194	-0.27	28.005	OCO	130.742
3	No ads	CH_4	0.116	-0.88	NA	HCH	108.556
						HCH	110.889
						HCH	107.988
						HCH	111.089
1		C	8.466	-6.780	24.864	NiCNi	92.625
1		CH	7.234	-6.430	12.496	NiCNi	86.953
						NiCH	128.159
						NiCH	127.646
2	No ads	CH_2	4.771	-4.010	18.984	HCH	104.459

1		CH_3	2.791	-1.910	46.123	HCH	108.625
						HCH	108.462
						HCH	109.137
2	No ads	CH_2OH	2.049	-1.540	NA	HCO	102.672
						COH	111.361
2		CHOH	3.984	-3.880	2.687	COH	109.150
						NiCO	129.418
2		CO	2.248	-2.090	7.553	NiCO	130.980
2		CH_3O	3.055	-2.630	16.144	HCH	112.982
						NiOC	100.484
2	No ads	CH_3OH	0.329	-0.300	NA	HCH	110.972
						COH	109.381
1		COOH	2.649	-2.260	17.199	OCO	117.096
						COH	104.002
1		H	3.589	-2.770	29.567	NiNiH	143.970
2		H_2	1.099	-0.220	399.480	NiNiH	143.545
						HNiH	61.125
1	No ads	H_2O	0.275	-0.290	NA	HOH	102.319
3		OH	3.774	-3.420	10.355	NiOH	113.419
1		CH_2O	1.090	-0.750	45.378	HCO	112.012
						HCH	112.984
1		O	7.059	-5.670	24.493	NiONi	85.523

These findings are needed to be compared with a reference of similar systems and geometry properties. The main two molecules to be taken into account are CH_4 and CO_2 and their angles are represented in table 12.

Table 12: CH_4 and CO_2 Angles in the Simulated System

# sim	Compound	Angle b/w	Simulation angle	Angle Literature	Difference
		N/A	o	o	%
H1	CO_2	OCO	130.742	180.000	27.366
3	CH_4	HCH	108.556	109.500	0.862
		HCH	110.889	109.500	1.268
		HCH	107.988	109.500	1.381
		HCH	111.089	109.500	1.451

In table 13, the bond lengths for CH_4 and CO_2 are shown and compared to literature values [27, 47]. It's essential to know the difference between the relaxed geometry of the molecules and within the simulated system. The stretched bonds may lead to dissociation or detaching an atom from its molecule.

Table 13: Bond Lengths of CH_4 and CO_2

Bond	Literature	Simulation	Difference
	Length (pm)		%
H-H	74.00	Broken	N/A
C-H	109.00	111.00	1.83
C-O	143.00	129.00	9.79
O-H	96.00	98.00	2.08
C=O	120.00	127.00	5.83

After dehydrogenation of CH_4 and obtaining the required barrier energy, hydrogen will be detached from it. That will lead to have a free hydrogen atom H and CH_3. Then, the dehydrogenation will continue till carbon deposits on the surface causing a deactivation of the catalyst. The deactivation of the catalyst has been mentioned

earlier and will be discussed when it comes to carbon adsorption. Meanwhile in this study, some of the main molecules that are related to CH_4 and CO_2 dissociations will be discussed in details separately and the rest will be referred to in the reaction network section.

5.4.1 CH_3 and CH_2

CH_3 adsorption energy is calculated to be 2.79 eV which is easier to be adsorbed on Ni surface than CH_4. It can be observed in figure 14 there is a bond formed between the carbon and the Ni surface. This adsorption is 46% higher than the literature [27, 47] for a relatively similar system. The formed bond C-Ni requires more energy to break than C-H and that will lead to easier detached of hydrogens from this molecule. In figure 15, it can be observed there was no adsorption detected for CH_2 molecule. There was deforming of the Ni surface and that may be caused by breaking the C-Ni bond.

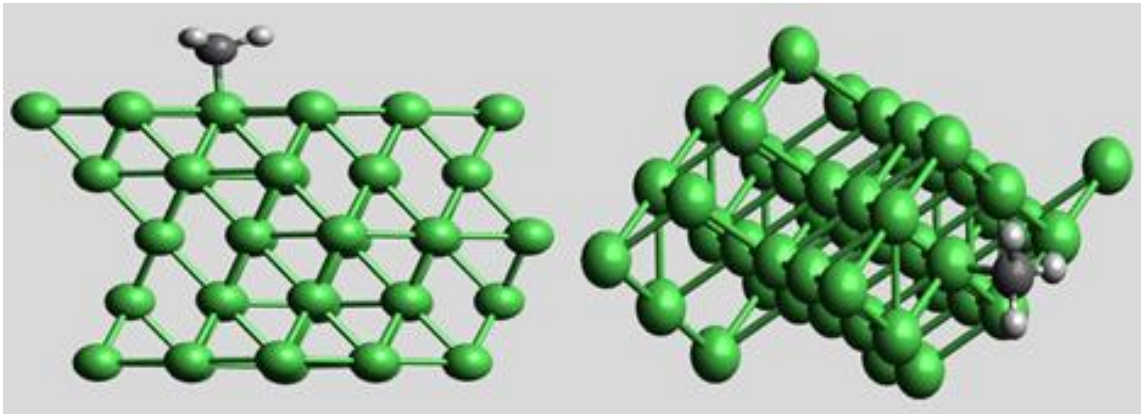

Figure 14: CH_3 Adsorption on Ni111

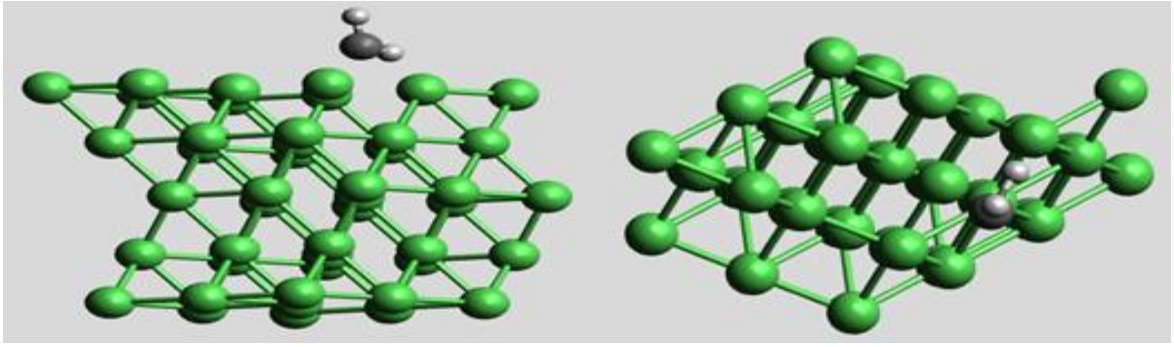

Figure 15: CH_2 Adsorption on Ni111

5.4.2 CH

As it can be observed in figure 16 that CH has been adsorbed forming a C-Ni bond and the adsorption energy was found to be 7.23 eV. This energy is about 12.50% higher than the literature [27, 47] – different number of layers. With every hydrogen has been detached from the original, the energy of adsorption is increasing. In this study, only the forward reaction has been taken into consideration and to fully understand the whole picture both reactions should be studied as there are many breaking and forming bonds will be occurring at the same time. Later on, the total network of reactions will be discussed in this study.

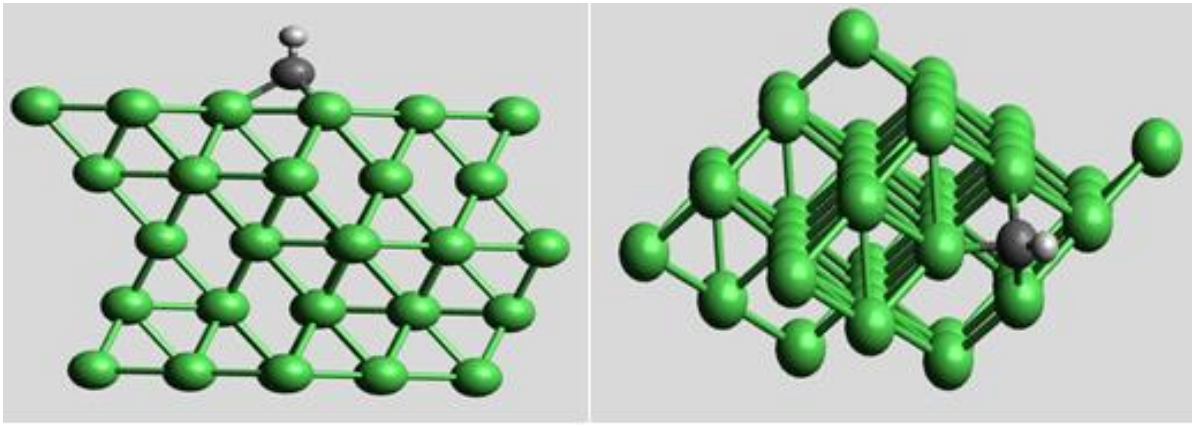

Figure 16: CH Adsorption on Ni111

5.4.3 Carbon (C)

Carbon can deposit on the surface due to many reactions paths. It could be due to CH_4 or CO_2 dissociations. The dehydrogenating of CH and CO dissociation are two possible ways to form C. The adsorption energy of C on the surface was found to be around 8.47 eV and it is higher than the other steps of the CH_4 dissociation and it can be observed in figure 17. This high energy indicates that Ni111 has a higher carbon resistivity than other surfaces have been mentioned earlier. This is undesired step and it deactivates the catalyst. This C can form CO molecule by being attached with free oxygen in the system as CO is one of the targeted molecules to be produced from this process. Depending on the concentration of the free oxygen, C can react to produce CO or deposit on the surface and inactive the catalyst. The formation of C from CO_2 dissociation was discussed earlier in this study.

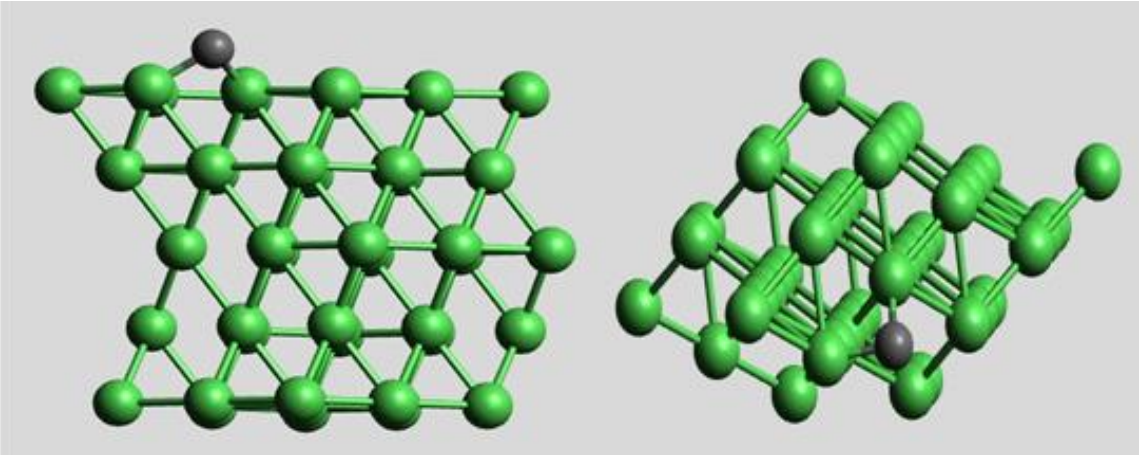

Figure 17: Carbon Adsorption on Ni111

5.4.4 CH_2O and CH_2OH

This is a transitional molecule and it is not stable and there are many pathways to form this molecule. One of these ways is to CH_2 reacts with free oxygen or by dehydrogenation of CH_2OH. The adsorption energy is found to be 1.09 eV and it is higher by 45% than literature [27, 47] and it can be seen in figure 18. Since it is a transitional molecule, the two ways reactions should be considered and that concentration of the system has a major effect on the adsorption energy and the geometry of the molecule. CH_2O can dissociate to CHO and free hydrogen or form CH_2OH by reacting with free H [27]. CH_2OH is formed by reacting CH_2O with free H and it is adsorbed on the surface with 2.05 eV as adsorption energy and it is represented in figure 19. It has been noted that C-Ni bond is always generated when

there is an adsorption occurs. In CH_2O adsorption there was Ni-O bond was formed beside C-Ni bond and this will eases the detaching atoms from the molecule.

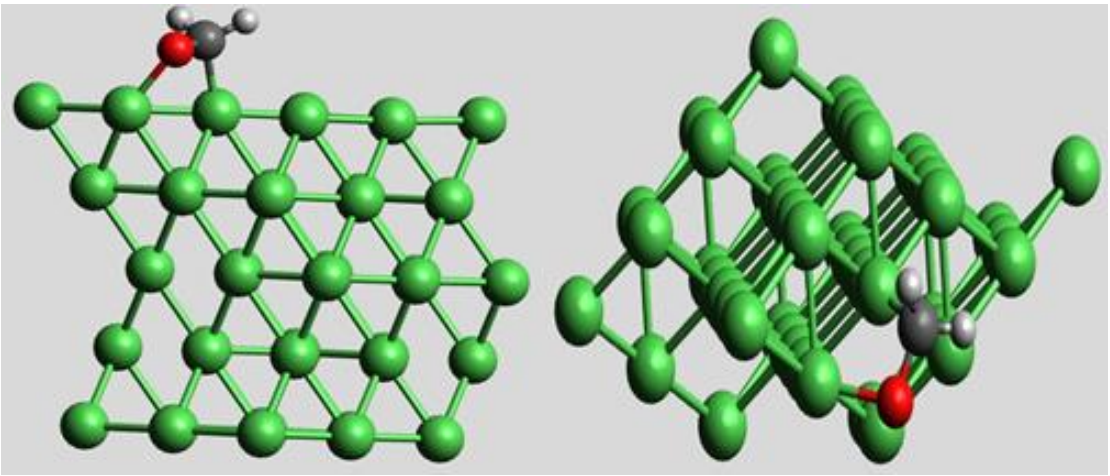

Figure 18: CH_2O Adsorption on Ni111

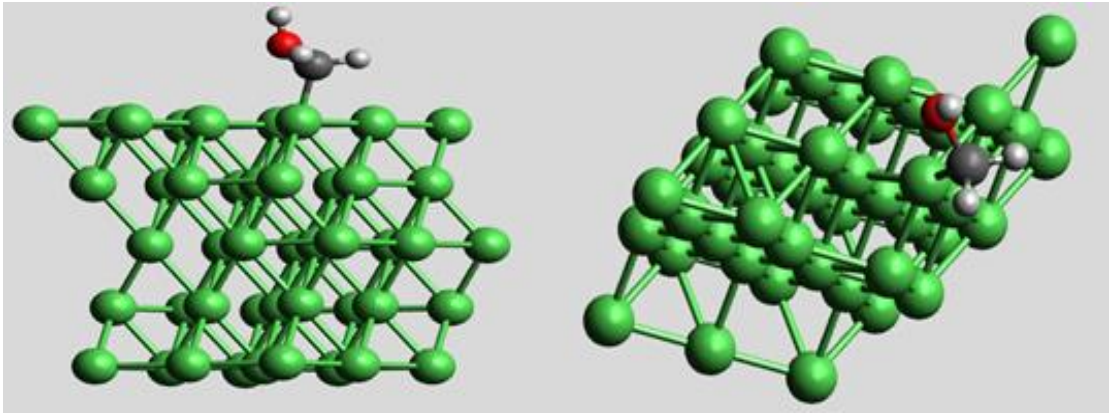

Figure 19: CH_2OH Adsorption on Ni1111

5.4.5 CHOH

The adsorption of CHOH is formed by dissociating into COH and detached a H as it can be seen in figure 20. The adsorption energy was calculated to be 3.98 eV which is higher than literature [27, 47] by around 2.7%. Forming of CHOH molecule could be by dehydrogenation of CH_2OH, reacting OH molecule with CH or different pathway.

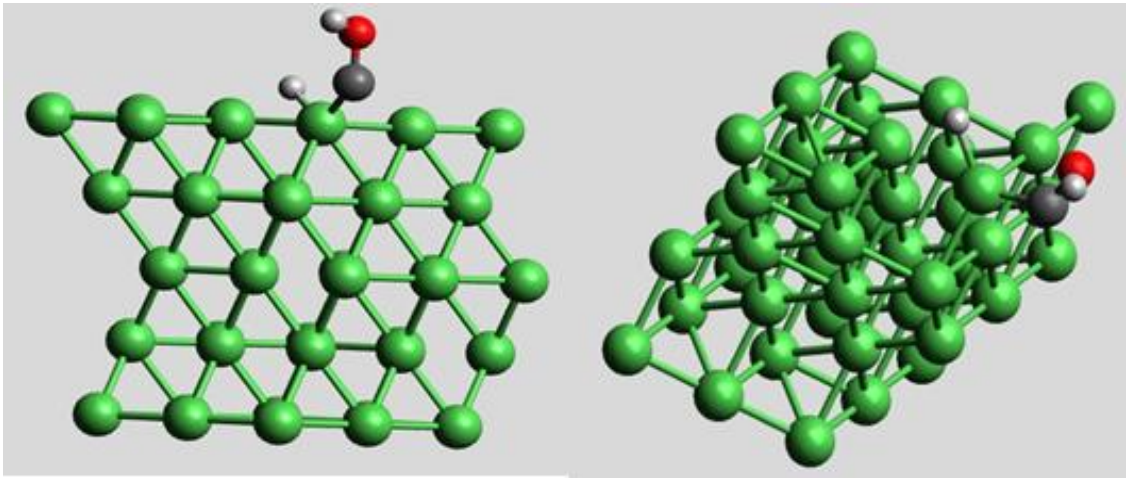

Figure 20: CHOH Adsorption on Ni111

5.4.6 CH_3O

In this molecule, it can be observed clearly in figure 21 that there was an adsorption and hydrogen atom was detached from the molecule and that will form CH_2O molecule adsorbed on the surface. The adsorption energy was found to be 3.05 eV. The adsorption and dissociation of CH_2O has been discussed earlier in this study.

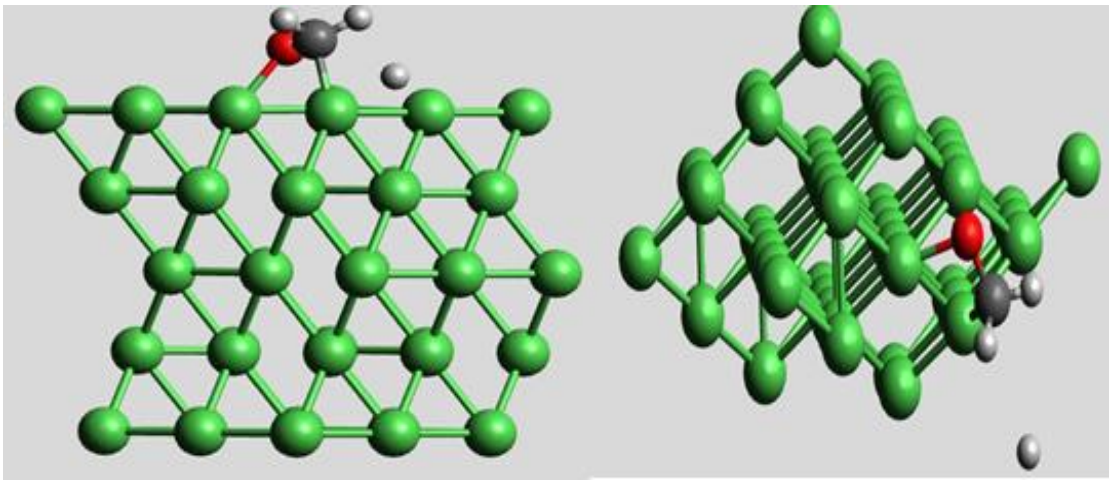

Figure 21: CH_3O Adsorption on Ni111

5.4.7 CH_3OH

CH_3OH adsorption on the surface requires around 0.33 eV which is slightly higher than the literature [27, 47] which was calculated to be 0.30 eV. In this study, CH3OH was not adsorbed on the surface as in figure 22 and it may require different concentration and distance to occur. The dissociation of CH_3OH would produce most of the transitional molecules of form of CH_xOH and CH_xO where ($0<x<3$). These transitional molecules where discussed earlier.

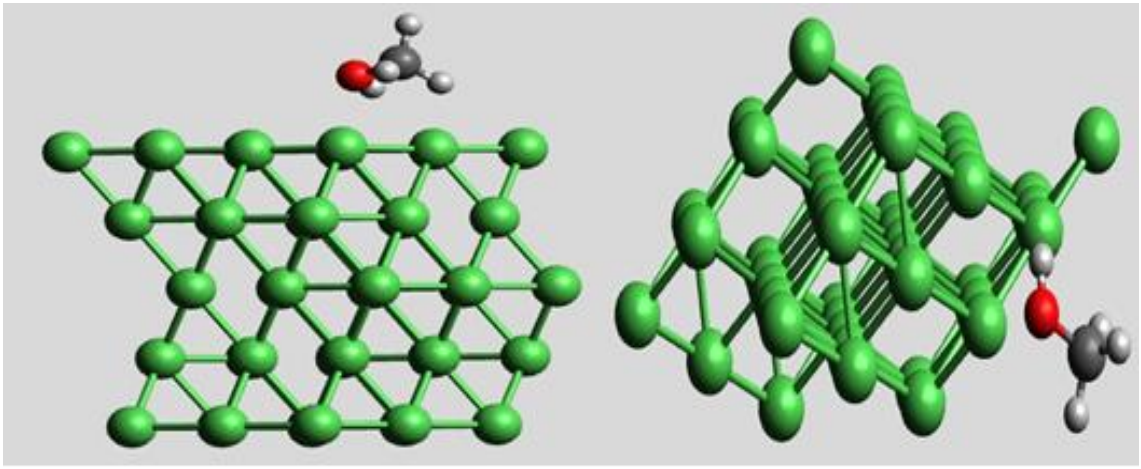

Figure 22: CH_3OH Adsorption on Ni111

5.4.8 COOH

COOH was adsorbed on the surface forming a C-Ni bond as it appears in figure 23 and the energy of this adsorption was calculated to be about 2.65 eV. This intermediate molecule can be formed by reacting free hydrogen atom or H_2 with CO_2 before dissociating into CO and OH or into CO and H_2O, respectively [26, 27].

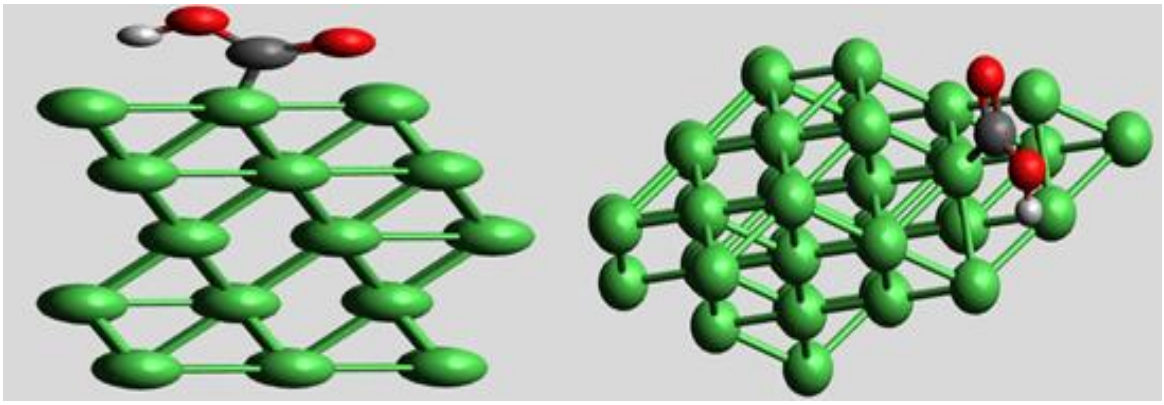

Figure 23: COOH Adsorption on Ni111

5.4.9 CO

CO is a linear mole with triple bonding between the two atoms. The oxidation of CH_4 and CO_2 dissociation will lead to form CO. In figure 24, the adsorption of CO can be seen and C-Ni bond was formed and the triple bond was reduced to double bond. The adsorption energy was calculated to 2.25 eV which is around 7.55% higher than the literature [27, 47]. The angle of the linear molecule was changed to 131^{o} due to the adsorption energy. CO can be formed from the transition molecules dehydrogenation such as COH and CHO. Reactivating of Ni surface can lead to form CO by oxidizing C from the surface.

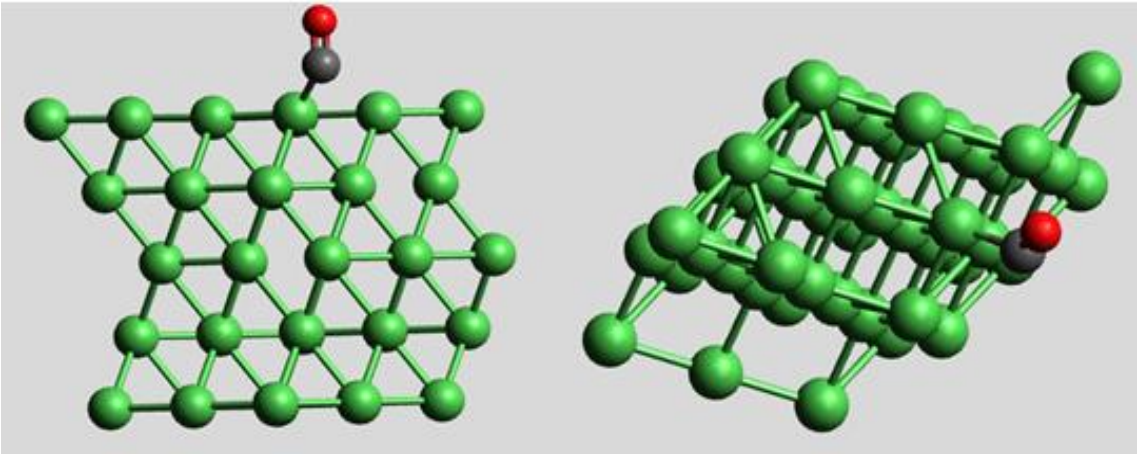

Figure 24: CO Adsorption on Ni111

5.5 Reactions Network

This predicted reactions network in figure 25 shows the mechanism of DRM on Ni surface taking into consideration the forward and backward reactions. It shows the dissociation of CH_4 and CO_2, the transitional molecules and side reactions. In order to fully understand the kinetic of DRM, this network has to be studied and calculate the required energy to obtain it as well as the reaction rates of these reactions. The orientation of the placed molecules on the surface of Ni has a major effect on the adsorption energies and how the bonds are formed. Most of these bonds are covalent bonds which are formed during the chemisorption of CO_2 on the surface. The initial distance of the molecules from the surface affects the physisorption energy and therefore, it this distance should be well chosen. There are many transitional

molecules that can be formed and the concentration of the radicalized atom or molecules could determine the last dissociation step. Some of these molecules have been discussed earlier in this study to better understanding of the reaction pathway of DRM. Findings in this study agree with literature in many of the molecules dissociation and the differences could be due to many reasons. These anticipated reasons are; the number of layers that were used to perform this study, distance from the surface and the concentration on the surface of the catalyst. In order to achieve reasonable mechanism of DRM, different active sites should be investigated. In this study, it was clear that for the same molecule being placed on different sites, gave different adsorption energies and some molecules were not adsorbed on some other sites.

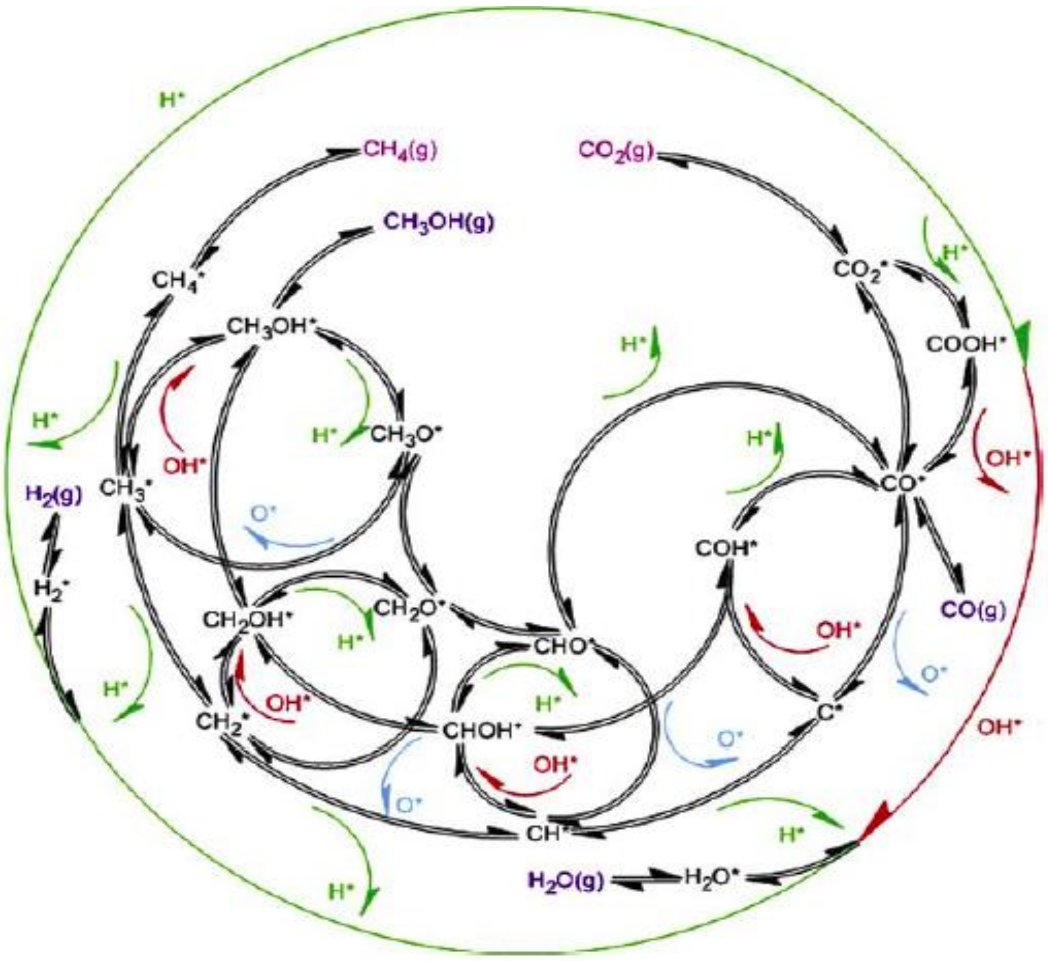

Figure 25: Predicted Reaction Network of DRM on Ni[27].

Chapter6 Conclusions

This study shows the greenhouse gases effects and role in the global warming phenomena and endangering the ecosystem. The main focus was on CO_2 and that due to its high emissions and its major role in global warming. Different technologies are used in order to capture and reform CO_2 have been investigated in this study. Moreover, different metals and surfaces were investigated to choose the optimum surface to perform DFT calculations.

DFT calculations were carried on using SIESTA simulation package using PBE-GGA functional. The simulated system consists of 45 Ni atoms (5 layers) and molecules were placed on top of the surface 2-3 Angstroms away. These simulations used 32 cores for each and counterpoise correction was applied to improve the accuracy of these calculations. SIESTA has proven its accuracy for systems that have less than 200 atoms and gives accurate data with a reasonable computational time.

DFT calculations were performed on Ni111 after screening a lot of metals aiming to better understand and calculating of adsorption energy of DRM. CH_4 and CO_2 dissociations are the main reactions and they were investigated on different sites using different orientations. The horizontal CO_2 molecules with a distance of 2 Angstrom from the surface has given better results and more favorable with a reasonable adsorption energy. The adsorption energy of CO_2 on the surface was calculated to be 0.194 eV and the OCO angle was around 131^o.

However, for CH_4 only physisorption has occurred and no chemisorption was detected for all the selected sites and that can be observed in the change of the geometry of the molecule. This indicates the first adsorption of CH_4 on the surfaces is the rate-determining step for its dissociation pathway and as overall for the reaction. The dissociation processes will generate carbon atoms that are deposited on the surface of Ni and that cause deactivation of the catalyst and the atomic O may oxidize the C to regenerate the surface. However, the transitional molecules play a major role on the reaction pathway of CH_4 and CO_2 dissociations and they were studied in order to understand possible reactions and molecules behavior on the surface of Ni.

In order to better understand the DRM process, it is required to study the forward and backward reactions network. This will give more information about the kinetics of this process and the possible step-determining reaction. Moreover, different concentrations of molecules are needed to study the concentration effect on the adsorption energies of the system.

This study claims that Ni-based catalysts are the optimum (especially Ni111) to carry on with DRM based on the many factors such as availability, cost of processing and resistivity of carbon deposition. More studies are required to verify these claims and come up with the optimum geometry of the catalyst as the future work will suggest.

Future Work

These following points should be considered to enhance this study:

- Study atom in a molecule (AIM) analysis with a different software (underway) and determine bond critical points, electron density and Laplacian of electron density.
- We shall study reduced density gradient (RDG) of the system and generate 3-d iso--surface map for how the entire system interact with the gas molecule) and display both weak vdW forces as well as strong H-bond forces.
- Considering Ni111 alloys
- Studying different layers and surfaces of Ni
- Detailed study of reaction mechanism and rate-determining steps
- Carbon deposition mechanism study in details.

References

[1] T. R. Anderson, E. Hawkins, and P. D. Jones, "CO2, the greenhouse effect and global warming: from the pioneering work of Arrhenius and Callendar to today's Earth System Models," *Endeavour,* vol. 40, no. 3, pp. 178-187, 2016.

[2] E. E. Agency, "CO2 Levels over years," ed: https://www.eea.europa.eu/data-and-maps/figures/atmospheric-concentration-of-co2-ppm-1/image_xlarge, 2010.

[3] *Greenhouse Gas (GHG) Emissions, US Environmental Protection Agency (http://www.epa.gov/ghgemissions),* 2017.

[4] R. S. Haszeldine, "Carbon Capture and Storage: How Green Can Black Be?," *Science,* vol. 325, no. 5948, pp. 1647-1652, 2009.

[5] D. Aaron and C. Tsouris, "Separation of CO2 from Flue Gas: A Review," *Separation Science and Technology,* vol. 40, no. 1-3, pp. 321-348, 2005/01/01 2005.

[6] B. Metz, O. Davidson, H. de Coninck, M. Loos, and L. Meyer, *Special Report on Carbon Dioxide Capture and Storage*. Cambridge Univ. Press, Cambridge, 2005.

[7] *International Energy Outlook 2016, US Energy Information Administration (http://www.eia.gov/outlooks),* 2017.

[8] M. E. Boot-Handford *et al.*, "Carbon capture and storage update," *Energy & Environmental Science,* 10.1039/C3EE42350F vol. 7, no. 1, pp. 130-189, 2014.

[9] S. Chu and A. Majumdar, "Opportunities and challenges for a sustainable energy future," *Nature,* 10.1038/nature11475 vol. 488, no. 7411, pp. 294-303, 08/16/print 2012.

[10] U. Ahmed, U. Zahid, Y. S. Jeong, C.-J. Lee, and C. Han, "IGCC process intensification for simultaneous power generation and CO2 capture," *Chemical Engineering and Processing: Process Intensification,* vol. 101, pp. 72-86, 3// 2016.

[11] A. Awadallah-F and S. Al-Muhtaseb, "Carbon dioxide sequestration and methane removal from exhaust gases using resorcinol–formaldehyde activated carbon xerogel," (in English), *Adsorption*, vol. 19, no. 5, pp. 967-977, 2013/10/01 2013.

[12] A. H. Berger and A. S. Bhown, "Selection of Optimal Solid Sorbents for CO2 Capture Based on Gas Phase CO2 composition," *Energy Procedia*, vol. 63, no. 0, pp. 2092-2099, // 2014.

[13] J. H. Cavka, C. A. Grande, G. Mondino, and R. Blom, "High Pressure Adsorption of CO2 and CH4 on Zr-MOFs," *Industrial & Engineering Chemistry Research*, vol. 53, no. 40, pp. 15500-15507, 2014/10/08 2014.

[14] J. Chen, L. S. Loo, and K. Wang, "High-Pressure CO2 Adsorption on a Polymer-Derived Carbon Molecular Sieve," *Journal of Chemical & Engineering Data*, vol. 53, no. 1, pp. 2-4, 2008/01/01 2008.

[15] M. A. Gonzalez-Salazar *et al.*, "Comparison of Current and Advanced Post-Combustion CO2 Capture Technologies for Power Plant Applications," *Energy Procedia*, vol. 23, pp. 3-14, // 2012.

[16] K. K. Amara *et al.*, "Dynamic Structural Evolution of Metal–Metal Bonding Network in Monolayer WS2," *Chemistry of Materials*, vol. 28, no. 7, pp. 2308-2314, 2016.

[17] W. L. Theo, J. S. Lim, H. Hashim, A. A. Mustaffa, and W. S. Ho, "Review of pre-combustion capture and ionic liquid in carbon capture and storage," *Applied Energy*, vol. 183, no. Supplement C, pp. 1633-1663, 2016/12/01/ 2016.

[18] H. Gerbelová, M. van der Spek, and W. Schakel, "Feasibility Assessment of CO2 Capture Retrofitted to an Existing Cement Plant: Post-combustion vs. Oxy-fuel Combustion Technology," *Energy Procedia*, vol. 114, no. Supplement C, pp. 6141-6149, 2017/07/01/ 2017.

[19] T. T. Journal, "**A pre-combustion capture system** ", ed: https://triz-journal.com/wp-content/uploads/library/graphics/2007-09-dmac03.GIF, 2007.

[20] E. S. Rubin, "Post Combustion to Capture CO2," ed: http://elements.geoscienceworld.org/content/gselements/4/5/311/F2.large.jpg, 2008.

[21] T. N. E. T. L. (NETL), "Oxy-fuel system to capture CO2," ed: https://www.netl.doe.gov/research/coal/carbon-storage/carbon-storage-faqs/co2-capture-process, Retrieved 2017.

[22] D. Moreira and J. C. M. Pires, "Atmospheric CO2 capture by algae: Negative carbon dioxide emission path," *Bioresource Technology*, vol. 215, no. Supplement C, pp. 371-379, 2016/09/01/ 2016.

[23] M. Kumar, S. Sundaram, E. Gnansounou, C. Larroche, and I. S. Thakur, "Carbon dioxide capture, storage and production of biofuel and biomaterials by bacteria: A review," *Bioresource Technology*, 2017/09/08/ 2017.

[24] L. HOWSTUFFWORKS.COM, "How Algae Biodiesel Works: A Bioreactor System," ed: HOWSTUFFWORKS.COM, 2008.

[25] N. MacDowell *et al.*, ed.

[26] J. Ko, B.-K. Kim, and J. W. Han, "Density Functional Theory Study for Catalytic Activation and Dissociation of CO2 on Bimetallic Alloy Surfaces," *The Journal of Physical Chemistry C*, vol. 120, no. 6, pp. 3438-3447, 2016.

[27] Y.-A. Zhu, D. Chen, X.-G. Zhou, and W.-K. Yuan, "DFT studies of dry reforming of methane on Ni catalyst," *Catalysis Today*, vol. 148, no. 3–4, pp. 260-267, 2009.

[28] Q. Yi, W. Li, J. Feng, and K. Xie, "Carbon cycle in advanced coal chemical engineering," *Chemical Society Reviews*, vol. 44, no. 15, pp. 5409-5445, 2015.

[29] M. Sigl, M. Bradford, H. Knozinger, and M. Vannice, "CO2 Reforming of methane over vanadia-promoted Rh/SiO2 catalysts," *Top Catalysts,* vol. 8, no. 3-4, pp. 211-222, 1999.

[30] J. R. Rostrupnielsen and J. H. B. Hansen, "CO2-Reforming of Methane over Transition Metals," *Journal of Catalysis,* vol. 144, no. 1, pp. 38-49, 1993/11/01/ 1993.

[31] A. M. Gadalla and B. Bower, "The role of catalyst support on the activity of nickel for reforming methane with CO2," *Chemical Engineering Science,* vol. 43, no. 11, pp. 3049-3062, 1988/01/01/ 1988.

[32] J. H. Edwards and A. M. Maitra, "The chemistry of methane reforming with carbon dioxide and its current and potential applications," *Fuel Processing Technology,* vol. 42, no. 2, pp. 269-289, 1995/04/01/ 1995.

[33] S. T. Oyama, P. Hacarlioglu, Y. Gu, and D. Lee, "Dry reforming of methane has no future for hydrogen production: Comparison with steam reforming at high pressure in standard and membrane reactors," *International Journal of Hydrogen Energy,* vol. 37, no. 13, pp. 10444-10450, 2012/07/01/ 2012.

[34] L. Zhang, X. Wang, X. Shang, M. Tan, W. Ding, and X. Lu, "Carbon dioxide reforming of methane over mesoporous nickel aluminate/γ-alumina composites," *Journal of Energy Chemistry*.

[35] P. N. ST. C. TEUNER, F. VON LINDE, "CO through CO2 reforming - The Calcor standard and Calcor economy processes," ed: *Oil Gas-European Magazine*, 2001, pp. 44-46.

[36] N. R. Udengaard, J.H.B. Hansen, D.C. Hanson, and J.A. Stal, vol. 90, ed: Oil & Gas Journal, 1992, pp. 62-67.

[37] Z. Alipour, M. Rezaei, and F. Meshkani, "Effect of Ni loadings on the activity and coke formation of MgO-modified Ni/Al2O3 nanocatalyst in dry reforming of methane," *Journal of Energy Chemistry*, vol. 23, no. 5, pp. 633-638, 2014.

[38] Y.-M. Dai, C.-Y. Lu, and C.-J. Chang, "Catalytic activity of mesoporous Ni/CNT, Ni/SBA-15 and (Cu, Ca, Mg, Mn, Co)-Ni/SBA-15 catalysts for CO2 reforming of CH4," *RSC Advances*, vol. 6, no. 77, pp. 73887-73896, 2016.

[39] S. De, J. Zhang, R. Luque, and N. Yan, "Ni-based bimetallic heterogeneous catalysts for energy and environmental applications," *Energy & Environmental Science*, vol. 9, no. 11, pp. 3314-3347, 2016.

[40] X. Fang *et al.*, "Dry reforming of methane on active and coke resistant Ni/Y2Zr2O7 catalysts treated by dielectric barrier discharge plasma," *Journal of Energy Chemistry*, vol. 25, no. 5, pp. 825-831, 2016.

[41] R. K. Singha *et al.*, "Synthesis of highly coke resistant Ni nanoparticles supported MgO/ZnO catalyst for reforming of methane with carbon dioxide," *Applied Catalysis B: Environmental*, vol. 191, pp. 165-178, 2016.

[42] I. H. Son *et al.*, "Study on coke formation over Ni/γ-Al2O3, Co-Ni/γ-Al2O3, and Mg-Co-Ni/γ-Al2O3 catalysts for carbon dioxide reforming of methane," *Fuel*, vol. 136, pp. 194-200, 2014.

[43] M. Usman and W. M. A. Wan Daud, "An investigation on the influence of catalyst composition, calcination and reduction temperatures on Ni/MgO catalyst for dry reforming of methane," *RSC Advances*, vol. 6, no. 94, pp. 91603-91616, 2016.

[44] L. Foppa, M.-C. Silaghi, K. Larmier, and A. Comas-Vives, "Intrinsic reactivity of Ni, Pd and Pt surfaces in dry reforming and competitive reactions: Insights from first

principles calculations and microkinetic modeling simulations," *Journal of Catalysis,* vol. 343, pp. 196-207, 2016.

[45] S. Arora and R. Prasad, "An overview on dry reforming of methane: strategies to reduce carbonaceous deactivation of catalysts," *RSC Advances,* vol. 6, no. 110, pp. 108668-108688, 2016.

[46] L. A. Schulz *et al.*, "On the coke deposition in dry reforming of methane at elevated pressures," *Applied Catalysis A: General,* vol. 504, pp. 599-607, 2015.

[47] Z. Wang, X. M. Cao, J. Zhu, and P. Hu, "Activity and coke formation of nickel and nickel carbide in dry reforming: A deactivation scheme from density functional theory," *Journal of Catalysis,* vol. 311, pp. 469-480, 2014.

[48] M. S. Aw, M. Zorko, I. G. Osojnik Črnivec, and A. Pintar, "Progress in the Synthesis of Catalyst Supports: Synergistic Effects of Nanocomposites for Attaining Long-Term Stable Activity in CH4–CO2 Dry Reforming," *Industrial & Engineering Chemistry Research,* vol. 54, no. 15, pp. 3775-3787, 2015.

[49] B. Kumar *et al.*, "New trends in the development of heterogeneous catalysts for electrochemical CO2 reduction," *Catalysis Today,* vol. 270, pp. 19-30, 2016.

[50] J. Niu, X. Du, J. Ran, and R. Wang, "Dry (CO2) reforming of methane over Pt catalysts studied by DFT and kinetic modeling," *Applied Surface Science,* vol. 376, pp. 79-90, 2016.

[51] J. Baltrusaitis and W. L. Luyben, "Methane Conversion to Syngas for Gas-to-Liquids (GTL): Is Sustainable CO2 Reuse via Dry Methane Reforming (DMR) Cost Competitive with SMR and ATR Processes?," *ACS Sustainable Chemistry & Engineering,* vol. 3, no. 9, pp. 2100-2111, 2015.

[52] W. Donphai, T. Witoon, K. Faungnawakij, and M. Chareonpanich, "Carbon-structure affecting catalytic carbon dioxide reforming of methane reaction over Ni-carbon composites," *Journal of CO2 Utilization,* vol. 16, pp. 245-256, 12// 2016.

[53] F. Guo, W. Jia, B. Hou, and Y. Zhang, "Dry re-forming of methane to synthesis gas over lignite semicokes catalyst at high pressure," *Energy Reports,* vol. 2, pp. 163-170, 11// 2016.

[54] Y. Kathiraser, U. Oemar, E. T. Saw, Z. Li, and S. Kawi, "Kinetic and mechanistic aspects for CO2 reforming of methane over Ni based catalysts," *Chemical Engineering Journal,* vol. 278, pp. 62-78, 2015.

[55] F. Polo-Garzon, M. He, and D. A. Bruce, "Ab initio derived reaction mechanism for the dry reforming of methane on Rh doped pyrochlore catalysts," *Journal of Catalysis,* vol. 333, pp. 59-70, 2016.

[56] S. Wang, G. Q. Lu, and G. J. Millar, "Carbon Dioxide Reforming of Methane To Produce Synthesis Gas over Metal-Supported Catalysts: State of the Art," *Energy & Fuels,* vol. 10, no. 4, pp. 896-904, 1996.

[57] A. Wolfbeisser, O. Sophiphun, J. Bernardi, J. Wittayakun, K. Föttinger, and G. Rupprechter, "Methane dry reforming over ceria-zirconia supported Ni catalysts," *Catalysis Today,* vol. 277, Part 2, pp. 234-245, 2016.

[58] J. Vicente, C. Montero, J. Ereña, M. J. Azkoiti, J. Bilbao, and A. G. Gayubo, "Coke deactivation of Ni and Co catalysts in ethanol steam reforming at mild temperatures in a fluidized bed reactor," *International Journal of Hydrogen Energy,* vol. 39, no. 24, pp. 12586-12596, 2014.

[59] Y. K. Han, C.-I. Ahn, J.-W. Bae, A. R. Kim, and G. Y. Han, "Effects of Carbon Formation on Catalytic Performance for CO2 Reforming with Methane on Ni/Al2O3

Catalyst: Comparison of Fixed-Bed with Fluidized-Bed Reactors," *Industrial & Engineering Chemistry Research,* vol. 52, no. 37, pp. 13288-13296, 2013.

[60] M. Usman and W. M. A. W. Daud, "Recent advances in the methanol synthesis via methane reforming processes," *RSC Advances,* vol. 5, no. 28, pp. 21945-21972, 2015.

[61] X. Yu, F. Zhang, and W. Chu, "Effect of a second metal (Co, Cu, Mn or Zr) on nickel catalysts derived from hydrotalcites for the carbon dioxide reforming of methane," *RSC Advances,* vol. 6, no. 74, pp. 70537-70546, 2016.

[62] J. Zhang and F. Li, "Coke-resistant Ni@SiO2 catalyst for dry reforming of methane," *Applied Catalysis B: Environmental,* vol. 176–177, pp. 513-521, 2015.

[63] B. Sarkar, R. Goyal, C. Pendem, T. Sasaki, and R. Bal, "Highly nanodispersed Gd-doped Ni/ZSM-5 catalyst for enhanced carbon-resistant dry reforming of methane," *Journal of Molecular Catalysis A: Chemical,* vol. 424, pp. 17-26, 2016.

[64] M. M. Barroso Quiroga and A. E. Castro Luna, "Kinetic Analysis of Rate Data for Dry Reforming of Methane," *Industrial & Engineering Chemistry Research,* vol. 46, no. 16, pp. 5265-5270, 2007.

[65] C. E. Quincoces and M. G. Gonzalez, "Kinetic Study on CO2 Reforming of Methane," *Journal of Chemical Engineering,* vol. 9, pp. 190-195, 2001.

[66] A. ERDOHELYI, J. CSERENYI , and F. SOLYMOSI, "Activation of CH4 and Its Reaction with CO2 over Supported Rh Catalysts," *Journal of Catalysis,* vol. 141, pp. 287-299, 1993.

[67] F. Polo-Garzon, J. K. Scott, and D. A. Bruce, "Microkinetic model for the dry reforming of methane on Rh doped pyrochlore catalysts," *Journal of Catalysis,* vol. 340, pp. 196-204, 2016.

[68] L. C. Grabow, A. a. Gokhale, S. T. Evans, J. a. Dumesic, and M. Mavrikakis, "Mechanism of the Water Gas Shift Reaction on Pt: First Principles, Experiments, and Microkinetic Modeling," vol. 12, pp. <p class="MsoListParagraph" style="margin-bottom:0in;margin-bottom:.0001pt; mso-add-space:auto;text-indent:-.25in;line-height:normal;mso-list:l0 level1 lfo1; mso-layout-grid-align:none;text-autospace:none"> 4608 − 4617., 2008.

[69] M. M. V. M. Souza, O. R. M. Neto, and M. Schmal, "Synthesis Gas Production from Natural Gas on Supported Pt Catalysts," *Journal of Catalysis,* vol. 15, pp. 21-27, 2006.

[70] T. Chagas *et al.*, "Room temperature observation of the correlation between atomic and electronic structure of graphene on Cu(110)," *RSC Advances,* vol. 6, no. 100, pp. 98001-98009, 2016.

[71] J. Krause, D. Borgmann, and G. Wedler, "Photoelectron Spectroscopic Study of the Adsorption of Carbon Dioxide on Cu(110) and Cu(110)K as Compared with the Systems Fe(110)CO2 and Fe(110)K + CO2," *Surf. Sci.,* pp. 1-10, 1996.

[72] J. Nakamura, J. A. Rodriguez, and C. T. Campbell, "Does CO2 Dissociatively Adsorb on Cu Surfaces?," *J. Phys.: Condens. Matter* vol. 1, pp. 140-160, 1989.

[73] U. Burghaus, "Surface Chemistry of CO2 − Adsorption of Carbon Dioxide on Clean Surfaces at Ultrahigh Vacuum," *Prog. Surf. Sci,* vol. 2, p. 161 − 217, 2014.

[74] F. T. B. Solymosi, "Structure and Reactions of CO2 Adsorbed on Clean and Promoted Metal Surfaces," *J. Mol. Catal,* vol. 2, p. 337 − 358, 1991.

[75] A. Goeppert, M. Czaun, J.-P. Jones, G. K. Surya Prakash, and G. A. Olah, "Recycling of carbon dioxide to methanol and derived products - closing the loop," *Chemical Society Reviews,* vol. 43, no. 23, pp. 7995-8048, 2014.

[76] C. Wang *et al.*, "Coking and deactivation of a mesoporous Ni–CaO–ZrO2 catalyst in dry reforming of methane: A study under different feeding compositions," *Fuel,* vol. 143, pp. 527-535, 2015.

[77] A. H. Bhrawy and M. A. Zaky, "An improved collocation method for multi-dimensional space–time variable-order fractional Schrödinger equations," *Applied Numerical Mathematics,* vol. 111, pp. 197-218, 2017.

[78] D. W. Blaylock, T. Ogura, W. H. Green, and G. J. O. Beran, "Computational Investigation of Thermochemistry and Kinetics of Steam Methane Reforming on Ni(111) under Realistic Conditions," *The Journal of Physical Chemistry C,* vol. 113, no. 12, pp. 4898-4908, 2009.

[79] J. Neugebauer and M. Scheffler, "Adsorbate-Substrate and Adsorbate-Adsorbate Interactions of Na and K Adlayers on Al(111)," *Phys. Rev. B: Condens. Matter Mater. Phys.*, p. 16067 − 16080., 1992.

[80] H. Atashi, J. Gholizadeh, F. Farshchi Tabrizi, J. Tayebi, and S. A. H. Seyed Mousavi, "Thermodynamic analysis of carbon dioxide reforming of methane to syngas with statistical methods," *International Journal of Hydrogen Energy*.

[81] L. C. S. Kahle *et al.*, "Methane Dry Reforming at High Temperature and Elevated Pressure: Impact of Gas-Phase Reactions," *Industrial & Engineering Chemistry Research,* vol. 52, no. 34, pp. 11920-11930, 2013.

[82] A. L. Karemore, P. D. Vaidya, R. Sinha, and P. Chugh, "On the dry and mixed reforming of methane over Ni/Al2O3 – Influence of reaction variables on syngas production," *International Journal of Hydrogen Energy*.

[83] S. A. Theofanidis, V. V. Galvita, H. Poelman, and G. B. Marin, "Enhanced Carbon-Resistant Dry Reforming Fe-Ni Catalyst: Role of Fe," *ACS Catalysis*, vol. 5, no. 5, pp. 3028-3039, 2015.

[84] W. Yang and D. He, "Role of poly(N-vinyl-2-pyrrolidone) in Ni dispersion for highly-dispersed Ni/SBA-15 catalyst and its catalytic performance in carbon dioxide reforming of methane," *Applied Catalysis A: General*, vol. 524, pp. 94-104, 8/25/ 2016.

[85] F. Huang, R. Wang, C. Yang, H. Driss, W. Chu, and H. Zhang, "Catalytic performances of Ni/mesoporous SiO2 catalysts for dry reforming of methane to hydrogen," *Journal of Energy Chemistry*, vol. 25, no. 4, pp. 709-719, 2016.

[86] E. C. Lovell, A. Fuller, J. Scott, and R. Amal, "Enhancing Ni-SiO2 catalysts for the carbon dioxide reforming of methane: Reduction-oxidation-reduction pre-treatment," *Applied Catalysis B: Environmental*, vol. 199, pp. 155-165, 12/15/ 2016.

[87] N. A. Pechimuthu, K. K. Pant, and S. C. Dhingra, "Deactivation Studies over Ni−K/CeO2−Al2O3 Catalyst for Dry Reforming of Methane," *Industrial & Engineering Chemistry Research*, vol. 46, no. 6, pp. 1731-1736, 2007.

[88] M. A. Vasiliades, M. M. Makri, P. Djinović, B. Erjavec, A. Pintar, and A. M. Efstathiou, "Dry reforming of methane over 5 wt% Ni/Ce1-xPrxO2-δ catalysts: Performance and characterisation of active and inactive carbon by transient isotopic techniques," *Applied Catalysis B: Environmental*, vol. 197, pp. 168-183, 11/15/ 2016.

[89] U. Olsbye, T. Wurzel, and L. Mleczko, "Kinetic and Reaction Engineering Studies of Dry Reforming of Methane over a Ni/La/Al2O3 Catalyst," *Industrial & Engineering Chemistry Research,* vol. 36, no. 12, pp. 5180-5188, 1997.

[90] Y. Chen and D. G. Vlachos, "Density Functional Theory Study of Methane Oxidation and Reforming on Pt(111) and Pt(211)," *Industrial & Engineering Chemistry Research,* vol. 51, no. 38, pp. 12244-12252, 2012.

[91] J. Ren, C.-F. Huo, J. Wang, Z. Cao, Y.-W. Li, and H. Jiao, "Density functional theory study into the adsorption of CO2, H and CHx (x = 0–3) as well as C2H4 on α-Mo2C(0 0 0 1)," *Surface Science,* vol. 600, no. 11, pp. 2329-2337, 2006.

[92] G.-C. Wang *et al.*, "Cluster and Periodic DFT Calculations of Adsorption and Activation of CO2 on the Cu(hkl) Surfaces," *Surf. Sci,* p. 205 − 217, 2004.

[93] J. M. Boereboom, R. Potestio, D. Donadio, and R. E. Bulo, "Toward Hamiltonian Adaptive QM/MM: Accurate Solvent Structures Using Many-Body Potentials," *Journal of Chemical Theory and Computation,* vol. 12, no. 8, pp. 3441-3448, 2016/08/09 2016.

[94] C. E. Woodward and J. Forsman, "A Many-Body Hamiltonian for Nanoparticles Immersed in a Polymer Solution," *Langmuir,* vol. 31, no. 1, pp. 22-26, 2015/01/13 2015.

[95] E. E. Dahlke and D. G. Truhlar, "Electrostatically Embedded Many-Body Expansion for Simulations," *Journal of Chemical Theory and Computation,* vol. 4, no. 1, pp. 1-6, 2008/01/01 2008.

[96] N. C. Costa, J. P. Lima, and R. R. dos Santos, "Spiral magnetic phases on the Kondo Lattice Model: A Hartree–Fock approach," *Journal of Magnetism and Magnetic Materials,* vol. 423, pp. 74-83, 2017.

[97] N. M. El-Metwaly and M. G. El-Ghalban, "Hartree-Fock, molecular docking, spectral, kinetic and antitumor considerations for cobalt, nickel, palladium and platinum (II)-bis carbothiohydrazide complexes," *Journal of Molecular Liquids,* vol. 220, pp. 265-276, 2016.

[98] C. A. Jiménez-Hoyos, T. M. Henderson, and G. E. Scuseria, "Generalized Hartree–Fock Description of Molecular Dissociation," *Journal of Chemical Theory and Computation,* vol. 7, no. 9, pp. 2667-2674, 2011.

[99] M. J. G. Peach, A. M. Teale, T. Helgaker, and D. J. Tozer, "Fractional Electron Loss in Approximate DFT and Hartree–Fock Theory," *Journal of Chemical Theory and Computation,* vol. 11, no. 11, pp. 5262-5268, 2015.

[100] G. Klepac, U. Maulik, and P. Dutta, "Chapter 12 - The Schrödinger equation as inspiration for a client portfolio simulation hybrid system based on dynamic Bayesian networks and the REFII model A2 - Bhattacharyya, Siddhartha," in *Quantum Inspired Computational Intelligence*Boston: Morgan Kaufmann, 2017, pp. 391-416.

[101] J. Zhai and B. Zheng, "On the local well-posedness for the nonlinear Schrödinger equation with spatial variable coefficient," *Journal of Mathematical Analysis and Applications,* vol. 445, no. 1, pp. 81-96, 2017.

[102] S. website, "SIESTA," ed.

[103] V. Verdinelli, A. Juan, J. M. Marchetti, and E. German, "A microscopic level insight into Pt doped TiZn (001) surface for hydrogen energy storage usage," *RSC Advances,* vol. 6, no. 77, pp. 73566-73575, 2016.

[104] D. Cheng, F. R. Negreiros, E. Apra ` , and Fortunelli, "A. Computational Approaches to the Chemical Conversion of Carbon Dioxide," vol. 6, p. 944 − 965, 2013.

[105] A. Iomin, "Quantum continuous time random walk in nonlinear Schrödinger equation with disorder," *Chaos, Solitons & Fractals,* vol. 93, pp. 64-70, 2016.

[106] J. O. Weidong Wu and L. C. Ahmed Al-Ostaz, "Applying Periodic Boundary Conditions in Finite Element Analysis," *SIMULIA Community Conference,* 2014.

[107] C. M. University. *Model Box Periodic Boundary Conditions - P.B.C.* Available: http://isaacs.sourceforge.net/phys/pbc.html

[108] A. Vakhrushev, "Schematic representation of the idea of periodic boundary conditions," ed. https://www.researchgate.net/profile/Alexander_Vakhrushev/publication/277813683/figure/fig4/AS:294321208217601@1447183052051/Figure-4-Periodic-boundary-conditions.png.

[109] R. C. Catapan, A. A. M. Oliveira, Y. Chen, and D. G. Vlachos, "DFT Study of the Water–Gas Shift Reaction and Coke Formation on Ni(111) and Ni(211) Surfaces," *The Journal of Physical Chemistry C,* vol. 116, no. 38, pp. 20281-20291, 2012.

[110] P. Haynes. (Ret. 2016). *The pseudopotential approximation*.

[111] A. S. Torralba, D. R. Bowler, T. Miyazaki, and M. J. Gillan, "Non-self-consistent Density-Functional Theory Exchange-Correlation Forces for GGA Functionals," *Journal of Chemical Theory and Computation,* vol. 5, no. 6, pp. 1499-1505, 2009.

[112] Emilio Artacho, "SIESTA Manual 4.0," J. D. G. Jose M. Cela, Alberto Garcia, Javier Junquera, Richard M. Martin, Pablo Ordejon, Daniel Sanchez-, Ed., ed, 2016.

Appendices

Appendix A: Excel calculations of the simulated system

Table 14: Adsorption Energy calculations for CO_2

	Ni111_1CO_2									
	Etot	cp1	cp2	cp3	cp4	cp5	cp6	Ecc	E_{ads}	Angle
H1	-45151.788	-44094.591	-1054.649	-44078.323	-1052.186	-44079.686	-1053.176	-2.354	0.194	130.740
H2	-45151.813	-44094.593	-1054.647	-44078.308	-1052.251	-44079.708	-1053.232	-2.380	0.193	131.590
H3	-45151.377	-44094.589	-1054.650	-44078.372	-1052.271	-44079.656	-1053.164	-2.178	-0.039	131.200
H4	-45151.759	-44094.593	-1054.649	-44078.364	-1051.942	-44079.777	-1052.944	-2.415	0.102	128.590
V1	-45150.013	-44094.594	-1054.646	-44078.301	-1054.641	-44078.778	-1055.171	-1.007	-0.234	179.310
V2	-45149.993	-44094.592	-1054.647	-44078.372	-1054.640	-44078.612	-1055.189	-0.790	-0.036	179.850
V3	-45149.892	-44094.593	-1054.646	-44078.399	-1054.639	-44078.717	-1055.193	-0.872	-0.219	179.510
V4	-45149.886	-44094.592	-1054.646	-44078.442	-1054.638	-44078.789	-1055.198	-0.907	-0.260	179.750

Table 15: Summary of adsorption energies of CO_2

Ni111_1CO_2		
Position	E_{ads} (eV)	Angle o
H1	0.194	130.74
H2	0.193	131.59
H3	-0.039	131.20
H4	0.102	128.59
V1	-0.234	179.31
V2	-0.036	179.85
V3	-0.219	179.51
V4	-0.260	179.75

Published		
Eads CO_2		Eads CO_2*
-0.27		-0.21

Table 16: Adsorption energy for CH_4 on different potential active sites

	Ni111_1CH_4									
	Etot	cp1	cp2	cp3	cp4	cp5	cp6	Ecc	E_{ads}	Angle
1	-44322.317	-44094.595	-226.586	-44078.378	-226.474	-44079.529	-226.606	-1.284	-0.148	108.556
2	-44322.317	-44094.595	-226.586	-44078.473	-226.498	-44002.839	-226.585	75.546	76.682	110.889
3	-44322.259	-44094.592	-226.586	-44078.511	-226.520	-44079.376	-226.620	-0.965	0.116	107.988
4	-44322.328	-44094.592	-226.586	-44078.511	-226.520	-44079.376	-226.620	-0.965	0.185	111.089

Table 17: Summary of adsorption and angles of CH_4

Ni111_1CH_4		
Position	E_{ads} (eV)	Angle
1	-0.148	108.556
2	76.682	110.889
3	0.116	107.988
4	0.185	111.089

Table 18: Adsorption energies for different molecules in the simulated system

	Ni111								
	Etot	cp1	cp2	cp3	cp4	cp5	cp6	Ecc	Eads
C_1	-44257.2	-44094.6	-152.131	-44078.3	-152.131	-44079.5	-152.978	-2.05483	8.4658
C_2	-44257.2	-44094.6	-152.131	-44078.3	-152.131	-44079.5	-152.984	-1.96857	8.489996
C_3	-44257.2	-44094.6	-152.131	-44078.4	-152.131	-44079.5	-152.978	-1.95638	8.574346
C_4	-44257.2	-44094.6	-152.131	-44078.4	-152.131	-44079.5	-152.978	-1.94178	8.580647
CH_1	-44274	-44094.6	-170.283	-44078.4	-170.249	-44079.6	-170.998	-1.92682	7.233513
CH_2	-44274.1	-44094.6	-170.286	-44078.4	-170.25	-44079.6	-170.999	-1.94543	7.245278
CH_3	-44274.1	-44094.6	-170.28	-44078.4	-170.25	-44079.5	-170.998	-1.8217	7.377294
CH_4	-44274.1	-44094.6	-170.287	-44078.5	-170.249	-44079.7	-170.997	-1.8715	7.344064
CH2_1	-44290.3	-44094.6	-188.601	-44078.3	-188.535	-44079.8	-189.158	-2.11102	4.980138
CH2_2	-44290.2	-44094.6	-188.6	-44078.4	-188.178	-44080	-188.797	-2.22717	4.771275
CH2_3	-44290.2	-44094.6	-188.601	-44078.5	-188.528	-44079.8	-189.15	-1.9436	5.098521
CH2_4	-44290.3	-44094.6	-188.6	-44078.4	-188.528	-44079.8	-189.153	-1.9794	5.13005
CH3_1	-44306.2	-44094.6	-207.438	-44078.4	-207.011	-44079.4	-207.356	-1.36291	2.790956
CH3_2	-44306.8	-44094.6	-207.438	-44078.4	-206.857	-44079.9	-207.242	-1.8606	2.878941
CH3_3	-44306.8	-44094.6	-207.438	-44078.5	-206.855	-44080	-207.241	-1.88366	2.838203
CH3_4	-44306.2	-44094.6	-207.439	-44078.5	-207.002	-44079.5	-207.349	-1.3399	2.805728
CH2OH_1	-44753	-44094.6	-653.87	-44078.4	-653.431	-44079.8	-654.038	-2.04865	2.471662
CH2OH_2	-44752.2	-44094.6	-653.863	-44078.4	-653.133	-44079.6	-653.637	-1.70792	2.048809
CH2OH_3	-44753.1	-44094.6	-653.859	-44078.4	-653.367	-44080.1	-653.966	-2.30205	2.358697
CH2OH_4	-44753	-44094.6	-653.868	-44078.4	-653.426	-44079.9	-654.031	-2.0984	2.461645

CHOH_1	-44736.9	-44094.6	-636.652	-44078.4	-636.512	-44079.9	-637.211	-2.20625	3.40704
CHOH_2	-44737.8	-44094.6	-636.64	-44078.4	-632.004	-44080.1	-632.92	-2.58426	3.984256
CHOH_3	-44736.9	-44094.6	-636.652	-44078.5	-636.531	-44079.9	-637.237	-2.18358	3.439681
CO_1	-44705.4	-44094.6	-606.601	-44078.5	-606.448	-44079.6	-607.208	-1.86826	2.314968
CO_2	-44705.4	-44094.6	-606.601	-44078.5	-606.453	-44079.7	-607.216	-1.95926	2.247867
CO_3	-44705.4	-44094.6	-606.602	-44078.4	-606.45	-44079.5	-607.211	-1.88963	2.306926
CH3O_1	-44753.9	-44094.6	-653.461	-44078.4	-650.074	-44080.2	-651.006	-2.74734	3.07731
CH3O_2	-44754	-44094.6	-653.461	-44078.4	-649.735	-44080.3	-650.77	-2.91339	3.054591
CH3O_3	-44754	-44094.6	-653.466	-44078.4	-649.894	-44080.3	-650.864	-2.85787	3.098907
CH3OH_1	-44769	-44094.6	-672.259	-44078.4	-672.1	-44080	-672.505	-2.07628	0.111594
CH3OH_2	-44769	-44094.6	-672.267	-44078.4	-672.145	-44079.8	-672.554	-1.84396	0.329132
CH3OH_3	-44769	-44094.6	-672.263	-44078.4	-672.156	-44079.7	-672.567	-1.72165	0.427031
COOH_1	-45167.9	-44095	-1067.96	-44078.4	-1067.68	-44079.8	-1068.59	-2.32093	2.648695
COOH_2	-45167.9	-44094.6	-1067.93	-44078.4	-1067.37	-44079.7	-1068.31	-2.29622	3.101233
COOH_3	-45168.1	-44094.6	-1067.96	-44078.4	-1067.56	-44079.8	-1068.5	-2.37551	3.134518
H_1	-44111.1	-44094.6	-12.2	-44078.4	-12.2	-44079	-12.3416	-0.71658	3.589007
H_2	-44111.6	-44094.6	-12.1998	-44078.4	-12.1998	-44078.8	-12.3789	-0.59311	4.208089
H_3	-44111.6	-44094.6	-12.2	-44078.4	-12.2	-44079	-12.3808	-0.75986	4.072101
H2_1	-44128.6	-44094.6	-31.2892	-44078.4	-25.0959	-44079.4	-25.4541	-1.37156	1.316704
H2_2	-44128.2	-44094.6	-31.2892	-44078.4	-26.8893	-44079.4	-27.1438	-1.2678	1.098857
H2_3	-44128.3	-44094.6	-31.2892	-44078.4	-27.0277	-44079.4	-27.2795	-1.2652	1.115284

H2O_1	-44574.5	-44094.6	-478.296	-44078.3	-478.237	-44079.3	-478.619	-1.30958	0.27464
H2O_2	-44574.5	-44094.6	-478.294	-44078.3	-478.234	---	---	44556.58	44558.16
H2O_3	-44574.5	-44094.6	-478.29	-44078.3	-478.239	---	---	44556.58	44558.19
OH_1	-44558.6	-44094.6	-458.585	-44078.4	-458.567	-44079	-459.424	-1.48347	3.93488
OH_2	-44558.6	-44094.6	-458.585	-44078.4	-458.566	-44079.1	-459.424	-1.63291	3.775969
OH_3	-44558.4	-44094.6	-458.586	-44078.4	-458.578	-44079.2	-459.319	-1.48261	3.774148
CO_1	-44705.4	-44094.6	-606.601	-44078.5	-606.448	-44079.6	-607.208	-1.86826	2.314968
CO_2	-44705.4	-44094.6	-606.601	-44078.5	-606.453	-44079.7	-607.216	-1.95926	2.247867
CO_3	-44705.4	-44094.6	-606.602	-44078.4	-606.45	-44079.5	-607.211	-1.88963	2.295892
CH2O_1	-44737.1	-44094.6	-639.164	-44078.4	-637.479	-44079.8	-638.316	-2.22215	1.090336
CH2O_2	-44736.6	-44094.6	-636.64	-44078.4	-636.209	-44079.7	-636.901	-2.00801	3.343391
CH2O_3	-44736.9	-44094.6	-636.652	-44078.5	-636.523	-44080	-637.235	-2.23604	3.370768
O_1	-44542.3	-44094.6	-438.946	-44078.2	-438.947	-44079	-439.905	-1.7406	7.058767
O_2	-44542.5	-44094.6	-438.947	-44078.4	-438.947	-44078.9	-439.906	-1.5322	7.409488
O_3	-44542.3	-44094.6	-438.947	-44078.3	-438.946	-44079	-439.908	-1.63579	7.152748

Table 19: Bond Lengths comparing between literature and simulation

Bond	Literature	Simulation	Difference
	Length (pm)		%
H-H	74.00	Broken	N/A
C-H	109.00	111.00	1.83
C-O	143.00	129.00	9.79
Ni-Ni	245.00	0.00	100.00
O-H	96.00	98.00	2.08
C=O	120.00	127.00	5.83

Table 20: Angles between atoms in molecules

# sim	Compound	Angle b/w	Simulation angle	Angle Literature	Difference
		N/A	o	o	%
H1	CO2	OCO	130.742	180.000	27.366
3	CH4	HCH	108.556	109.500	0.862
		HCH	110.889	109.500	1.268
		HCH	107.988	109.500	1.381
		HCH	111.089	109.500	1.451

Table 21: Overall findings from the simulated system

# sim	Remark	Compound	Ea Sim eV	Ea Literature eV	Error % %	Angle b/w N/A	Angle o
H1		CO2	0.194	-0.27	28.005	OCO	130.742
4	**No ads**	CH4	0.185	-0.880	**78.951**	HCH	108.556
						HCH	110.889
						HCH	107.988
						HCH	111.089
1		C	8.466	-6.780	24.864	NiCNi	92.625
1		CH	7.234	-6.430	12.496	NiCNi	86.953
						NiCH	128.159
						NiCH	127.646
2	No ads	CH2	4.771	-4.010	18.984	HCH	104.459
1		CH3	2.791	-1.910	46.123	HCH	108.625
						HCH	108.462
						HCH	109.137
2	No ads	CH2OH	2.049	-1.540	33.040	HCO	102.672
						COH	111.361

2		CHOH	3.984	-3.880	2.687	COH	109.150
						NiCO	129.418
2		CO	2.248	-2.090	7.553	NiCO	130.980
2		CH3O	3.055	-2.630	16.144	HCH	112.982
						NiOC	100.484
2	No ads	CH3OH	0.329	-0.300	9.711	HCH	110.972
						COH	109.381
1		COOH	2.649	-2.260	17.199	OCO	117.096
						COH	104.002
1		H	3.589	-2.770	29.567	NiNiH	143.970
2		H2	1.099	-0.220	**399.480**	NiNiH	143.545
						HNiH	61.125
1	No ads	H2O	0.275	-0.290	5.297	HOH	102.319
3		OH	3.774	-3.420	10.355	NiOH	113.419
1		CH2O	1.090	-0.750	45.378	HCO	112.012
						HCH	112.984
1		O	7.059	-5.670	24.493	NiONi	85.523

Table 22: Comparing adsorption energies between SIESTA and VASP

	Adsorption Energy (eV)	
Molecule	SIESTA	VASP
CO_2	-0.197	-0.27
CH4	-0.116	-0.020
C	-8.466	-6.780
CH	-7.234	-6.430
CH2	-4.771	-4.010
CH3	-2.791	-1.910
CH2OH	-2.049	-1.540
CHOH	-3.984	-3.880
CO	-2.248	-2.090
CH3O	-3.055	-2.630
CH3OH	-0.329	-0.300
COOH	-2.649	-2.260
H	-3.589	-2.770
H2	-1.099	-0.220
H2O	-0.275	-0.290
OH	-3.774	-3.420
CH2O	-1.09	-0.750
O	-7.059	-5.670

Appendix B: Simulations files

```
# System description
SystemLabel      Ni111_1CO2_H1
NumberOfAtoms    48
NumberOfSpecies  3

%block ChemicalSpeciesLabel
    1   28  Ni
    2    6  C
    3    8  O
%endblock ChemicalSpeciesLabel

#Coordintes from previous run
MD.UseStruct.File F

AtomicCoordinatesFormat NotScaledCartesianAng
%block AtomicCoordinatesAndAtomicSpecies
-0.000000000     -0.000000000      2.034689216  1
 7.475500000     -0.000000000      8.138452816  1
 1.245904207      0.719323130      0.000000000  1
 1.245904207      0.719323130      6.103763600  1
-0.000000000      1.438646259      4.069074384  1
 2.491808415     -0.000000000      2.034689216  1
 2.491808415     -0.000000000      8.138452816  1
 3.737787377      0.719323130      0.000000000  1
 3.737787377      0.719323130      6.103763600  1
 2.491808415      1.438646259      4.069074384  1
 4.983691585     -0.000000000      2.034689216  1
 4.983691585     -0.000000000      8.138452816  1
 6.229595792      0.719323130      0.000000000  1
 6.229595792      0.719323130      6.103763600  1
 4.983691585      1.438646259      4.069074384  1
-1.245904208      2.157969389      2.034689216  1
 6.229595792      2.157969389      8.138452816  1
-0.000000000      2.877292518      0.000000000  1
-0.000000000      2.877292518      6.103763600  1
-1.245941585      3.596680388      4.069074384  1
 1.245904207      2.157969389      2.034689216  1
 1.245904207      2.157969389      8.138452816  1
 2.491883170      2.877292518      0.000000000  1
 2.491883170      2.877292518      6.103763600  1
 1.245866830      3.596680388      4.069074384  1
 3.737787377      2.157969389      2.034689216  1
 3.737787377      2.157969389      8.138452816  1
 4.983691585      2.877292518      0.000000000  1
 4.983691585      2.877292518      6.103763600  1
 3.737750000      3.596680388      4.069074384  1
-2.491845793      4.316003517      2.034689216  1
-2.491845793      4.316003517      8.138452816  1
-1.245941585      5.035326647      0.000000000  1
```

```
#Functional
XC.functional    GGA
XC.Authors    PBE
MM.Grimme.S6 0.75
%block MM.Potentials # Dispersion correction using Grimme's method MODIFY HERE
1 1 Grimme    111.932       3.124     #    Nickel & Nickel
1 2 Grimme     45.057       3.014     #    Nickel & Carbon
1 3 Grimme     28.497       2.904     #    Nickel & Oxygen
2 2 Grimme     18.137       2.904     #    Carbon & Carbon
2 3 Grimme     11.471       2.794     #    Carbon & Oxygen
3 3 Grimme      7.255       2.684     #    Oxygen & Oxygen
%endblock MM.Potentials
#SCF
MaxSCFIterations 300
DM.Tolerance 0.001
DM.MixingWeight 0.01
DM.NumberPulay 8

#Cutoffs and k-grids
MeshCutoff    300.000000 Ry
MeshSubDivisions 6
kgrid_cutoff 12.0 Ang
%block kgrid_Monkhorst_Pack
  2  0  0  0.0
  0  2  0  0.0
  0  0  2  0.0
%endblock kgrid_Monkhorst_Pack
SolutionMethod diagon
#Structure relaxation
MD.TypeOfRun    CG
MD.VariableCell    false
MD.NumCGsteps    300
MD.MaxCGDispl 0.8 Bohr
#Charges
WriteMullikenPop 1
WriteHirshfeldPop true
WriteVoronoiPop true
SaveBaderCharge true
PartialChargesAtEveryGeometry true
#Output
WriteCoorXmol true
WriteCoorCerius true
WriteMDXmol true
#Output
WriteCoorXmol true
WriteCoorCerius true
WriteMDXmol true
```

Figure 26: SIESTA input file

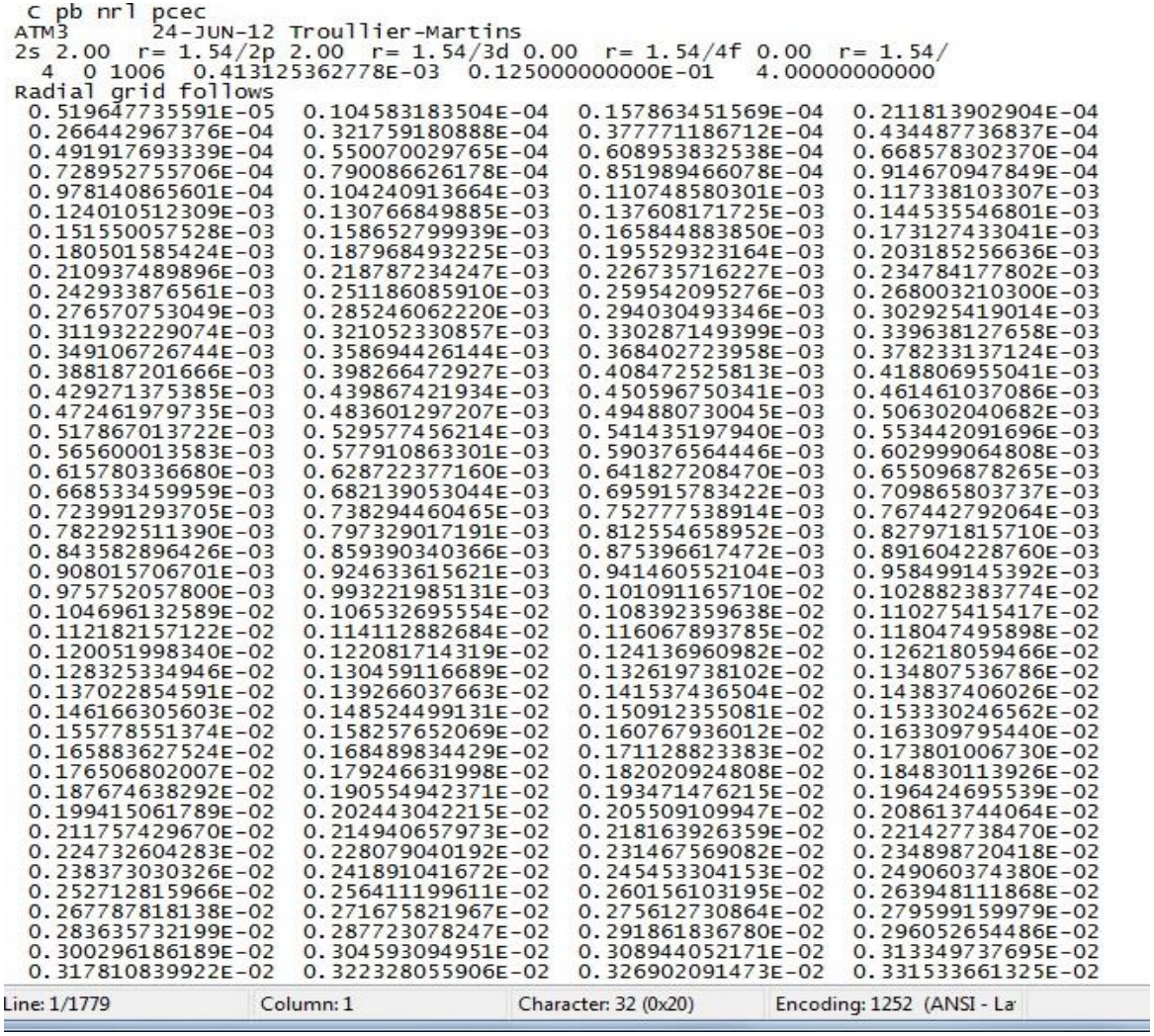

Figure 27: Example of pseudopotential file

```
#$ -cwd # current working directory
#$ -o 'salida_$JOB_ID.out' # output file
#$ -e salida_${JOB_ID}.err#
#$ -j yes # For merging stderr y stdout into a file
#$ -S /bin/bash # shell
#$ -q normal_haswell # queue name
#$ -pe impi 32 # parallel enviroment Intel MPI, 32 cores
#$ -V # exports all environmental variables
#$ -N Ni111_1CO2_H1_2CH4 # job name

#use module to load variables to be able to run mpi
module load siesta/siesta_3.2-pl-5

#Ejecucion run
time mpirun -n $NSLOTS /soft/haswell/siesta/3.2-pl-5/siesta <Ni111_1CO2_H1_2CH4.fdf> output
```

Figure 28: SIESTA run file

```
Siesta Version:                                          siesta-3.2-pl-5
Architecture  : x86_64-unknown-linux
Compiler flags: mpiifort -O2 -xHost -ip -mp1 -fpp -warn unused,truncated_source,uncalled,declarations,usage
PARALLEL version
NetCDF support

* Running on   32 nodes in parallel
>> Start of run:  29-DEC-2016  23:24:15

                           ************************
                           *  WELCOME TO SIESTA  *
                           ************************

reinit: Reading from standard input
************************** Dump of input data file ****************************
# System description
SystemLabel      Ni111_1CO2_H1_2CH4
NumberOfAtoms    58
NumberOfSpecies  4
%block ChemicalSpeciesLabel
    1   28  Ni
    2    6  C
    3    8  O
    4    1  H
%endblock ChemicalSpeciesLabel
#Coordintes from previous run
MD.UseStruct.File F
AtomicCoordinatesFormat NotScaledCartesianAng
%block AtomicCoordinatesAndAtomicSpecies
-0.000000000    -0.000000000     2.034689216  1
 7.475500000    -0.000000000     8.138452816  1
 1.245904207     0.719323130     0.000000000  1
 1.245904207     0.719323130     6.103763600  1
-0.000000000     1.438646259     4.069074384  1
 2.491808415    -0.000000000     2.034689216  1
 2.491808415    -0.000000000     8.138452816  1
 3.737787377     0.719323130     0.000000000  1
 3.737787377     0.719323130     6.103763600  1
 2.491808415     1.438646259     4.069074384  1
 4.983691585    -0.000000000     2.034689216  1
 4.983691585    -0.000000000     8.138452816  1
 6.229595792     0.719323130     0.000000000  1
 6.229595792     0.719323130     6.103763600  1
 4.983691585     1.438646259     4.069074384  1
-1.245904208     2.157969389     2.034689216  1
 6.229595792     2.157969389     8.138452816  1
-0.000000000     2.877292518     0.000000000  1
-0.000000000     2.877292518     6.103763600  1
-1.245941585     3.596680388     4.069074384  1
```

Line: 1/139304 | Column: 1 | Character: 83 (0x53) | Encoding: 1252 (ANSI - La

Figure 29: Example of SIESTA output file 1

```
timer:  cdiag4       130960       0.171   22335.950     1.63
timer:  c-eigvec      65480       6.460  423023.060    30.88
timer:  c-buildD      65480       1.416   92731.864     6.77
timer:  DHSCF4          438      13.919    6096.640     0.45
timer:  dfscf           438      12.600    5518.673     0.40
timer:  overfsm         438       0.242     105.894     0.01
timer:  optical           1       1.766       1.766     0.00


elaps: ELAPSED times:
elaps:  Routine       Calls   Time/call    Tot.time        %
elaps:  siesta            1   43845.500   43845.500   100.00
elaps:  Setup             1       3.066       3.066     0.01
elaps:  bands             1       0.001       0.001     0.00
elaps:  writewave         1       0.002       0.002     0.00
elaps:  KSV_init          1       0.011       0.011     0.00
elaps:  IterMD          438     100.093   43840.842    99.99
elaps:  hsparse         438       0.031      13.584     0.03
elaps:  overlap         438       0.010       4.427     0.01
elaps:  IterSCF        8185       5.124   41936.350    95.65
elaps:  kinefsm         876       0.010       8.751     0.02
elaps:  nlefsm          876       1.372    1202.043     2.74
elaps:  DHSCF          8624       1.281   11047.636    25.20
elaps:  DHSCF1            1       0.034       0.034     0.00
elaps:  DHSCF2          438       0.634     277.737     0.63
elaps:  REORD         69871       0.000       6.864     0.02
elaps:  POISON         9062       0.014     122.822     0.28
elaps:  DHSCF3         8624       1.197   10320.186    23.54
elaps:  rhoofd         8624       0.414    3571.712     8.15
elaps:  cellXC         8624       0.085     732.671     1.67
elaps:  vmat           8623       0.630    5436.226    12.40
elaps:  MolMec          876       0.005       4.782     0.01
elaps:  diagon         8185       3.610   29550.762    67.40
elaps:  c-eigval      65480       0.196   12842.102    29.29
elaps:  c-buildHS     65480       0.001      88.511     0.20
elaps:  cdiag        130960       0.199   26116.347    59.56
elaps:  cdiag1       130960       0.008    1057.391     2.41
elaps:  cdiag2       130960       0.060    7909.689    18.04
elaps:  cdiag3       130960       0.121   15855.328    36.16
elaps:  cdiag4       130960       0.005     716.427     1.63
elaps:  c-eigvec      65480       0.205   13435.872    30.64
elaps:  c-buildD      65480       0.049    3184.418     7.26
elaps:  DHSCF4          438       1.019     446.335     1.02
elaps:  dfscf           438       0.914     400.525     0.91
elaps:  overfsm         438       0.009       4.143     0.01
elaps:  optical           1       0.000       0.000     0.00

>> End of run:  30-DEC-2016  11:35:00
```

Figure 30: Example of SIESTA output file 2